

Compacted Concrete Pavement



January 2022
Final Report

Project number TR201904
MoDOT Research Report number cmr 22-001

PREPARED BY:

Kamal H. Khayat, Ph.D., P.Eng.

Nima Farzadnia, Ph.D.

Ahmed Abdelrazik, Ph.D.

Missouri University of Science and Technology

PREPARED FOR:

Missouri Department of Transportation

Construction and Materials Division, Research Section

TECHNICAL REPORT DOCUMENTATION PAGE

1. Report No. cmr 22-001	2. Government Accession No.	3. Recipient's Catalog No.	
4. Title and Subtitle Compacted Concrete Pavement		5. Report Date October 2021 Published: January 2022	
		6. Performing Organization Code	
7. Author(s) Kamal H. Khayat, Ph.D., P.Eng. http://orcid.org/0000-0003-1431-0715 Nima Farzadnia, Ph.D., https://orcid.org/0000-0002-9396-4102 Ahmed Abdelrazik, Ph.D., https://orcid.org/0000-0002-3075-5725		8. Performing Organization Report No.	
9. Performing Organization Name and Address Missouri University of Science and Technology Center for Infrastructure Engineering Studies 500 W. 16th St. Rolla, MO 65409-0710		10. Work Unit No.	
		11. Contract or Grant No. MoDOT project # 201904	
12. Sponsoring Agency Name and Address Missouri Department of Transportation (SPR-B) Construction and Materials Division P.O. Box 270 Jefferson City, MO 65102		13. Type of Report and Period Covered Final Report (September 2018-December 2021)	
		14. Sponsoring Agency Code	
15. Supplementary Notes Conducted in cooperation with the U.S. Department of Transportation, Federal Highway Administration. MoDOT research reports are available in the Innovation Library at https://www.modot.org/research-publications .			
16. Abstract The main objective of this project was to evaluate construction issues and characterize the long-term performance of compacted concrete pavement (CCP). Three CCP test cells were designed and constructed in Scott County, Missouri, as part of a larger construction project. The total pavement length was 42 ft for the three cells. Cell 1 and Cell 2 were prepared without fibers and had a length of 15 and 12 ft, respectively. Cell 3 was prepared with 5 lb/yd ³ (pcy) of synthetic fibers and had a length of 15 ft. The moisture content of the concrete was kept between 5% and 6%, and the water-to-cementitious material ratio was maintained between 0.31 and 0.38. Test results showed that the incorporation of fibers enhanced the mechanical properties (compressive and flexural strengths) of CCP mixtures when proper compaction was provided, as in the case of cast-in field samples. Also, fibers changed the flexural failure mode of saw-cut and cast-in-field CCP samples from brittle to ductile failure. The incorporation of fibers had a restraining effect on the drying shrinkage of CCP mixtures. The use of fibers did not have a significant effect on the performance of CCP mixtures, as shown from the falling weight deflectometer (FWD), truck loading tests and curling and warping. This can be mainly related to the extremely dry consistency of the CCP mixtures (Vebe consistency > 60) that can hinder bond strength in the interfacial transition zone with the matrix. This was more accentuated in the saw-cut samples from the paved CCP as the paving process in the field did not provide enough compaction. As for the size of slabs, results showed that the size of CCP slabs was more effective in the curling and warping measurements. The slab with longer length (15 ft) showed higher variations in curing and warping along the diagonal, transverse and longitudinal lengths over time. Therefore, the use of fibers in CCP can be recommended provided that the CCP mixture has adequate workability and sufficient compaction energy applied during construction.			
17. Key Words Compacted concrete pavement; Field implementation; Mechanical properties; Shrinkage; Durability		18. Distribution Statement No restrictions. This document is available through the National Technical Information Service, Springfield, VA 22161.	
19. Security Classif. (of this report) Unclassified.	20. Security Classif. (of this page) Unclassified.	21. No. of Pages 82	22. Price



Compacted Concrete Pavement

Project Number: TR201904

Final Report

Investigators

Kamal H. Khayat, Ph.D., P.Eng., Professor, Missouri S&T

Nima Farzadnia, Ph.D.

Ahmed Abdelrazik, Ph.D.

October 25, 2021

COPYRIGHT

The authors herein are responsible for the authenticity of their materials and for obtaining written permissions from publishers or individuals who own the copyright to any previously published or copyrighted material used herein.

DISCLAIMER

The opinions, findings, and conclusions expressed in this document are those of the investigators. They are not necessarily those of the Missouri Department of Transportation, the Minnesota Department of Transportation, or the Federal Highway Administration. This information does not constitute a standard or specification.

ACKNOWLEDGMENTS

The authors would like to acknowledge the financial support of the Missouri Department of Transportation (MoDOT) and the Centre for Infrastructure Engineering Studies (CIES) at Missouri S&T. The authors would like to thank Mrs. Jennifer Harper, P.E., PMP and Mr. John Donahue, P.E. from Missouri DOT for their technical assistance throughout this project. The assistance of Mr. Tom Burnham, P.E. and Mr. Michael Wallace from Minnesota Department of Transportation with the field data acquisition and analysis is greatly appreciated.

EXECUTIVE SUMMARY

To evaluate construction issues and characterize the long-term performance of compacted concrete pavement (CCP), three CCP test cells were designed and constructed in Scott County, Missouri, as part of a larger construction project. The three CCP cells were prepared with and without structural synthetic macro fibers (cells 1, 2, and 3). The total pavement length was 42 ft for the three cells. Cell 1 and Cell 2 were prepared with no fibers and had a length (i.e., distance between transverse joints) of 15 ft and 12 ft, respectively. Cell 3 was prepared with fibers and had a length of 15 ft. The width of the paved sections was fixed at 24 ft.

On October 24th, 2018, a test strip was paved in Scott County, Missouri. Constant surface alignment checks were performed, and the paver was adjusted as necessary. The Vebe consistency time and density of fresh compacted concrete were measured during the paving in compliance with ASTM C 1170. MoDOT also installed and instrumented sensors, including sensors to monitor strains due to variations in environmental conditions, dynamic load response, and joint openings. The sensors included a thermocouple tree, two joint opening block outs, vibrating wire strain gauges, and dynamic strain gauges.

Cast-in-field mixtures were prepared on the plant site at I-55 in Scott City on October 25, 2018. The fiber-reinforced and non-fiber-reinforced mixtures were tested for flexural properties using 18 prismatic molds measuring 6"x6"x24" and for compression strength using 18 cylindrical molds measuring 6"x12". Mixture 1 was used as the base mixture for the construction of Cells 1

and 2, while mixture 3 was prepared with 5 lb/yd³ (pcy) of synthetic fibers to replicate Cell 3. The moisture content of the CCP was kept between 5% and 6%, and the water-to-cementitious material ratio (w/cm) was maintained between 0.31 and 0.38. In order to maintain the proper curing moisture and temperature, wet burlaps were used to cover the samples, followed by plastic sheets and blankets. The samples were demolded and transported to Missouri S&T on October 29th. Transportation was carried out in accordance with ASTM C 31 with test samples cushioned in sand in boxes to prevent damage from jarring. Additionally, samples were wrapped in wet burlap to prevent moisture loss during transportation. The transportation time was limited to four hours.

The compressive strength test was conducted in compliance with ASTM C39. All cylinders were capped one day before the testing using high-strength Sulphur capping compound according to ASTM C 617. The flexural strength test was conducted on prismatic samples measuring 6"x6"x24" (span of 18") according to ASTM C1609. The rapid chloride ion permeability of samples measuring 4"x2" was evaluated for saw-cut samples in accordance with ASTM C1202. The surface electrical resistivity of samples was measured in accordance with AASHTO T95. The surface resistivity test method consisted of measuring the resistivity of 4"x6" core samples using a four-point Wenner probe array. Samples measuring 4"x1" cut from cores were prepared to determine the air-void system according to ASTM C 457. The freeze-thaw resistance of saw-cut samples was evaluated in accordance with ASTM C666, Procedure A. Deicing salt scaling test was carried out using three saw-cut slabs measuring 11"x10"x3" for Mixtures 1 and 2 in accordance with ASTM C672. Drying shrinkage was determined for saw-cut prisms measuring 3"x3"x11.3" according to ASTM C157 using a digital type extensometer (DEMEC gauge).

The compressive strength of a mixture containing 5 pcy fiber was found to be greater than that of samples made without fibers. The compressive strength of cast-in-field samples was found to be greater than that of saw-cut samples. For instance, the 91-d compressive strength of cast-in-field samples for Mixtures 1 and 2 was 41% and 39% greater than that of saw-cut specimens, respectively, indicating that the rate of compaction was greater for the cast-in-field samples than in paver-applied samples. Incorporating 5 pcy fiber increased flexural strength slightly in cast-in-field samples but decreased the flexural strength in saw-cut samples. For example, the use of fibers increased the flexural strength of cast-in-place samples from 555 to 685 psi and decreased the flexural strength of saw-cut specimens from 404 to 295 psi. The curing time, on the other hand, increased the flexural strength. As expected, the addition of 5 pcy fiber enhanced post-cracking behavior. Incorporating 5 pcy fiber increased the rapid chloride ion permeability by 35%. However, using 5 pcy fiber resulted in a decrease in bulk and surface electrical resistivity of 5% and 15%, respectively. Mixtures containing 5 pcy fiber had an entrapped air content of 5.1% compared to 4.0% for the plain mixture. The freezing and thawing properties of mixtures prepared with and without fiber were comparable. No visible scaling was observed after 80 cycles (30 cycles beyond the standard test method), hence indicating that the two mixtures can develop proper resistance to de-icing salt scaling. After 80 freeze-thaw cycles, the cumulative mass loss increased rapidly as the number of freeze-thaw cycles increased, resulting in visible surface degradation. The incorporation of 5 pcy fiber significantly reduced drying shrinkage. Drying shrinkage of the non-fibrous mixture was 1125 $\mu\epsilon$ compared to 900 $\mu\epsilon$ for the fiber-containing mixture.

The curling and warping measurements were conducted as per ASTM E1364 on December 19th, 2018, September 27th, 2019, and then September 16th, 2020. The CCP cells

(Cells 1, 2, and 3) were subjected to curling and warping measurements. The measurements were conducted in the longitudinal, transverse, and diagonal directions. Over time, the curling and warping of pavement sections increased. There was no discernible difference in deflection between the fiber-reinforced and unreinforced cells.

The falling weight deflectometer (FWD) was conducted on 16th of September 2020 by MoDOT. The test was used to measure the deformations at different locations from the loading plate. The analysis included the calculation of FWD deflection values as well as the load transfer efficiency (LTE) values derived from the readings of FWD at three different CCP slabs (Cell 1, Cell 2, and Cell 3). The deflection was measured using nine transducers with varying distances from the loading plate. The measurements were conducted under three loading rates of 80-81 psi, 107-109 psi, and 140-142 psi, respectively. The FWD was also used to determine the degree of interlock between adjacent slabs of the CCP. The FWD test results indicated that the deflection values in Cell 3 (CCP with fiber) were greater than those in the other two cells (without fibers). The increased deflection of Cell 3 could be a result of voids formed in the interfacial transition zone with the fibers or it could be a result of weaker subgrade support.

A truck loading test was conducted by Missouri S&T on cells 1, 2, and 3 to investigate the effect of fibers on performance of CCP. The cells were instrumented using a typical set of sensors embedded at various locations of the three stations. The sensors included dynamic strain gauges, two vibrating wire gauges aligned in the longitudinal and the transverse directions, as well as two thermocouples located at the top and the bottom of the CCP slab sections. The results of the truck loading tests cannot be conclusive due to the high mortality rate of the embedded sensors. However, when the speed was increased to 10 mph, the responsive sensors indicated that Cell 3 (CCP with fiber) had a relatively wider range of strain values (up to 60). Cell 3

exhibited a strain of 50 $\mu\epsilon$ under static load. These values were limited to 45 $\mu\epsilon$ for the various speed scenarios, while the strain in Cell 1 was 30 $\mu\epsilon$ under static load. The limited results obtained indicated that the use of 5 pcy of synthetic fibers had no discernible effect on the performance of the CCP slabs when dynamic loads were applied.

According to environmental data analysis, longitudinal and transverse strains decreased during the summer, reaching their lowest levels in the first week of July. Following that, the strains began to increase with the increase in ambient temperature. The transverse strain decreased at a much slower rate than the longitudinal strain. The results indicated that the use of fiber had no significant effect on the deformations caused by environmental variations during the reporting period. Generally the presence of fibers or the variation of the slab length from 12 to 15 ft did not have a significant effect on the environmental strain where the difference in the longitudinal and transverse strains at the three cells did not exceed 4% and 2%, respectively.

Keywords: Compacted concrete pavement, curling and warping, falling weight deflectometer, fiber-reinforced concrete, flexural behavior, pavement, truck loading.

Table of Contents

ACKNOWLEDGMENTS	1
EXECUTIVE SUMMARY	IV
1 INTRODUCTION	1
2 PROJECT OBJECTIVE.....	2
3 PROJECT OPERATION	4
3.1 TEST STRIP	4
3.2 INSTRUMENTATION.....	7
3.3 PAVING OPERATIONS	10
3.4 SAMPLING	11
4 PROJECT OPERATION	15
4.1 VEBE TEST (CONSISTENCY TIME AND DENSITY).....	15
4.2 COMPRESSIVE STRENGTH.....	16
4.3 FLEXURAL STRENGTH RESULTS.....	17
4.4 RAPID CHLORIDE ION PERMEABILITY TEST (RCPT).....	22
4.5 BULK/SURFACE ELECTRICAL RESISTIVITY	23
4.6 AIR-VOID SYSTEM.....	25
4.7 FREEZE-THAW RESISTANCE.....	26
4.8 DEICING SALT-SCALING RESISTANCE.....	28
4.9 DRYING SHRINKAGE	31
5 CELL PERFORMANCE.....	34
5.1 CURLING AND WARPING	34
5.2 FALLING WEIGHT DEFLECTOMETER	40
5.3 TRUCK LOADING TEST.....	50

5.4	ENVIRONMENTAL PERFORMANCE (ANALYSIS OF MNDOT DATA).....	57
6	CONCLUDING REMARKS.....	62
	REFERENCES.....	66

LIST OF FIGURES

<i>Figure 1. Project location: 587 State Hwy PP Scott City, MO 63780.....</i>	<i>4</i>
<i>Figure 2. Project location: 587 State Hwy PP Scott City, MO 63780.....</i>	<i>4</i>
<i>Figure 3. Surface adjustments</i>	<i>5</i>
<i>Figure 4. Density measurement.....</i>	<i>5</i>
<i>Figure 5. Density adjustments</i>	<i>6</i>
<i>Figure 6. Visual observation of the cross section.....</i>	<i>7</i>
<i>Figure 7. Instrumentation operation.....</i>	<i>7</i>
<i>Figure 8. Sensors and gauges applied in Cell 1, 2 and 3</i>	<i>8</i>
<i>Figure 9. Instrumentation schematics (plan).....</i>	<i>9</i>
<i>Figure 10. Loading process of the slip-form paving.....</i>	<i>10</i>
<i>Figure 11. Paving and adjustments</i>	<i>10</i>
<i>Figure 12. Finishing process.....</i>	<i>11</i>
<i>Figure 13. Location of the plant site: 800 Rose-Con Rd Scott City, MO 63780</i>	<i>11</i>
<i>Figure 14. Sampling of concrete.....</i>	<i>12</i>
<i>Figure 15. Vebe test apparatus for determining consistency/density of fresh CCP</i>	<i>12</i>
<i>Figure 16. Compaction tools and process.....</i>	<i>13</i>
<i>Figure 17. Sample curing and protection on site.....</i>	<i>13</i>
<i>Figure 18. Demolding and transportation of samples.....</i>	<i>14</i>
<i>Figure 19. Demolding and transportation of samples.....</i>	<i>14</i>
<i>Figure 20. Vebe test</i>	<i>16</i>
<i>Figure 21. Flexural strength test.....</i>	<i>18</i>
<i>Figure 22. Example of parameter calculations for first-peak load equal to peak load.....</i>	<i>19</i>
<i>Figure 23. Load-deflection curves of three field-cast prismatic samples of the two investigated mixtures at 7, 28, and 91 days.....</i>	<i>20</i>

Figure 24. Load-deflection curves of three saw-cut prisms of the two investigated mixtures at 91, 120, and 180 days..... 21

Figure 25. Testing apparatus for RCPT..... 23

Figure 26. Testing apparatus for surface resistivity (left) and bulk resistivity (right)..... 24

Figure 27. Sample preparation for air-void system analysis 25

Figure 28. Variations of relative dynamic modulus of elasticity of Mixture 1 (without fibers) and Mixture 2 (with fibers) determined on saw-cut samples 27

Figure 29. Variations of salt scaling mass loss of Mixture 1 (without fibers) and Mixture 2 (with fibers) determined on saw-cut samples..... 32

Figure 30. Drying shrinkage and mass loss measurement 32

Figure 31. Variations of drying shrinkage determined on saw-cut samples 33

Figure 32. Direction of measurements - longitudinal, diagonal, and transverse lengths. 34

Figure 33. Test setup and measuring equipment..... 35

Figure 34. Deflection of cell 1 made with fibers vs. cell 3 made without fibers (L=12 ft) measured on 12/19/18..... 37

Figure 35. Deflection of cell 1 made with fibers vs. cell 3 made without fibers (L=12 ft) measured on 09/27/19..... 37

Figure 36. Deflection of cell 1 made with fibers vs. cell 3 made without fibers (L=12 ft) measured on 09/16/20..... 38

Figure 37. Deflection (in.) of cells without fibers with L=12' (Cell 1) vs. L=15' (Cell 2) - 12/19/18 38

Figure 38. Deflection (in.) of cells without fibers with L=12' (Cell 1) vs. L=15' (Cell 2) - 09/27/19 39

Figure 39. Deflection (in.) of cells without fibers with L=12' (Cell 551) vs. L=15' (Cell 2) - 09/16/20 39

Figure 40. FWD equipment and schematic of loading plate and transducer location (drawing is adopted from Wang and Birken, 2014)..... 40

Figure 41. FWD Deflections at Cell 1 (Stress 80-81 psi)..... 41

Figure 42. LTE (%) at Cell 1 (Stress 80-81 psi)..... 42

Figure 43. FWD Deflections at Cell 1 (Stress 107-109 psi)..... 42

Figure 44. LTE (%) at Cell 1 (Stress 107-109 psi)..... 43

Figure 45. FWD Deflections at Cell 1 (Stress 140-142 psi)..... 43

Figure 46. LTE (%) at Cell 1 (Stress 140-142 psi)..... 44

Figure 47. FWD Deflections at Cell 2 (Stress 80-81 psi)..... 44

Figure 48. LTE (%) at Cell 2 (Stress 80-81 psi)..... 45

Figure 49. FWD Deflections at Cell 2 (Stress 107-109 psi)..... 45

Figure 50. LTE (%) at Cell 2 (Stress 107-109 psi)..... 46

Figure 51. FWD Deflections at Cell 2 (Stress 140-142 psi)..... 46

Figure 52. LTE (%) at Cell 2 (Stress 140-142 psi)..... 47

Figure 53. FWD Deflections at Cell 3 (Stress 80-81 psi)..... 47

Figure 54. LTE (%) at Cell 3 (Stress 80-81 psi)..... 48

Figure 55. FWD Deflections at Cell 3 (Stress 107-109 psi)..... 48

Figure 56. LTE (%) at Cell 3 (Stress 107-109 psi)..... 49

Figure 57. FWD Deflections at Cell 3 (Stress 140-142 psi)..... 49

Figure 58. LTE (%) at Cell 3 (Stress 140-142 psi)..... 50

Figure 59. Schematic of truckload configuration, dimensions in in. 51

Figure 60. Truck at the weigh station 52

Figure 61. Connection of sensors to jumper (picture shows connections for Cell 2)..... 53

Figure 62. Truck loading test 53

Figure 63. Measurement of the sensors' resistance prior to testing 54

Figure 64. Variations in strain during the truck movement – bottom part of Pavement (Cell 1 with fiber) 56

Figure 65. Variations in strain during the truck movement – bottom part of Pavement (Cell 3 with fiber) 56

Figure 66. Temperature readings of the thermistors attached to the top and bottom of the slab section at station 551 (Cell 1) 58

Figure 67. Temperature readings of the thermistors attached to the top and bottom of the slab section at station 552 (Cell 2) 58

Figure 68. Temperature readings of the thermistors attached to the top and bottom of the slab section at station 553 (Cell 3) 59

Figure 69. Temperature readings of the thermistors attached to the top and the bottom of the slab section at the three investigated stations..... 59

Figure 70. Strain variations at the longitudinal and the transverse directions of the three investigated stations 61

LIST OF TABLES

<i>Table 1. Typical characteristics of the three tested cells of CCP</i>	2
<i>Table 2. Experimental program</i>	3
<i>Table 3. Instrumented sensors in Cells 1, 2 and 3</i>	8
<i>Table 4. Vebe test results</i>	16
<i>Table 5. Compressive strength of samples</i>	17
<i>Table 6. Flexural and residual strength results</i>	22
<i>Table 7. RCPT scale for chlorides as per ASTM C1202</i>	23
<i>Table 8. RCPT results for saturated cores</i>	23
<i>Table 9. Bulk electrical resistivity of the two investigated mixtures (KΩ.cm)</i>	24
<i>Table 10. Surface electrical resistivity of two investigated mixtures (KΩ.cm)</i>	25
<i>Table 11. Air-void content and spacing factor of the two investigated mixtures</i>	26
<i>Table 12. Saw-cut slabs before and after exposure to salt scaling (80 cycles)</i>	28
<i>Table 13. Temperature and relative humidity data</i>	35
<i>Table 14. Axle weights and pressure at tire-pavement contact area (driver side)</i>	52
<i>Table 15. Resistance of sensors (CE001, CE002, CE003, and CE004) for Cells 1, 2, and 3</i>	54
<i>Table 16. Adjusted Data Acquisition System setting based on resistance of sensors</i>	55
<i>Table 17. Value ranges recorded for non-responsive sensors</i>	55

1 INTRODUCTION

Due to the increasing budget constraints and decreasing time in pavement construction, there has been renewed interest in exploring the application of cost-effective and rapid pavement construction techniques. Roller-compacted concrete (RCC) is a stiff mixture of aggregate, cementitious materials, and water, that is compacted by vibratory rollers [ACI 325, 1995]. Compacted concrete pavement (CCP) is an advanced form of RCC. The CCP is comprised of similar proportions as that of RCC; however, it utilizes an admixture that enables better finishing that can lead to durable surface texture. The major difference in construction is that CCP has a longer “fresh” or “green” period and requires little or no rolling that makes the riding surface more uniform and consistent. The use of CCP technology is supposed to secure smooth texture during paving.

Past research undertaken at the Missouri University of Science and Technology (Missouri S&T) in collaboration with the Missouri Department of Transportation (MoDOT) for the investigating of in-situ properties of RCC mixtures demonstrated prospective application in pavement construction with acceptable performance [Khayat and Libre, 2014]. However, limited experience exists with CCP. This project investigated the performance of CCP designed with special design features and durability of surface texture that can reduce construction cost and secure safe and durable surface texture. Of special interest in this project is the performance of CCP cells made with fiber-reinforced concrete (FRC) and the length of the pavement sections. A total of 5 pcy of structural synthetic macro fibers was used for the FRC, and the test sections were either 12 or 15 ft in length. Key fresh and hardened properties of the CCP mixtures were evaluated, and pavement quality after construction was monitored periodically.

2 PROJECT OBJECTIVE

In order to assess the construction issues and characterize the long-term performance of the proposed CCP technology, three CCP test cells made with and without fiber as part of a larger project that were constructed in Scott County, Missouri. Table 1 shows the typical characteristics of the three tested cells of CCP with different panel sizes that were prepared with and without structural synthetic macro fibers (Cells 1, 2, and 3). The total pavement length was 42 ft for the three cells. Cell 1 and Cell 2 were prepared with no fibers and had a length of 15 ft and 12 ft, respectively. Cell 3 was prepared with fibers and had a length of 15 ft. The total pavement width was fixed at 24 feet.

Table 1. Typical characteristics of the three tested cells of CCP

Item	Cell 1	Cell 2	Cell 3
Mixture	Control CCP	Control CCP	Fiber-reinforced CCP
Fiber content (%)	0	0	Minimum 20% (ASTM C1609)
Length (ft)	500	500	250
Panel size (WxLxT)	24 ft × 15 ft × 6 in.	24 ft × 12 ft × 6 in.	24 ft × 15 ft × 6 in.
Joint size (in.)	0.125 in. × T/4	0.125 in. × T/4	0.125 in. × T/4

The study aimed at determining the performance of CCP mixtures. The primary performance characteristics included mechanical properties, drying shrinkage, durability, and enhancement of joint load transfer gained from fiber-reinforcement of the pavement. The various field and laboratory research tasks that were undertaken by Missouri S&T are elaborated below. Table 2 summarizes the testing program that was conducted in this proposed research.

Table 2. Experimental program

Evaluated performance	Cell 1 or 2	Cell 3	Samples	Test method
Construction/instrumentation				
Install sensors	x	x		
Sampling preparation				
Cut samples from additional 15-ft sections	x	x		
Create research test samples from fresh concrete during pavement construction	x	x		ASTM C1435
Lab testing of saw-cut and cored samples				
	No. of samples	No. of samples		
Compressive strength (7, 28, 56 d) (N = 3)	9	9	3 × 6" cores	ASTM C39
Flexural strength of CCP without fiber (7, 28, 56 d) (N = 3)	9		6 × 6 × 22" prisms	ASTM C78
Flexural strength of FRC (7, 28, 56 d) (N = 3)		9	6 × 6 × 22" prisms	ASTM C1609
Freeze-thaw durability (N = 3)	3	3	3 × 4 × 16" prisms	
Hardened air content and spacing factor (N = 2)	3	3	Part of 4" cores (4 × 1")	ASTM C457
56-d permeability RCPT (N = 3)	3	3	Part of 4" cores (4 × 2")	ASTM C1202
Deicer salt scaling (N = 2)	2	2	11 × 10 × 3" slabs	ASTM C 672
Bulk resistivity (N = 2)	2	2	4" cores	ASTM C1760
Drying shrinkage (after 7 d moist curing, 180 d dry curing) (N = 3)	3	3	3×3× 11.3" prisms	ASTM C 157
Total no. of samples	34	34		
Lab testing of samples prepared during pavement construction				
Compressive strength (7, 28, 56 d) (N = 3)	6-9	6-9	6 × 12" Cylinders	ASTM C39
Flexural strength of CCP without fiber (7, 28, 56 d) (N = 3)	6-9		6 × 6 × 22" prisms	ASTM C78
Flexural strength of FRC (7, 28, 56 d) (N = 3)		6-9	6 × 6 × 22" prisms	ASTM C1609
Coefficient of thermal expansion (N = 3)	3	3	4 × 8" cylinders	
Total no. of samples	Up to 21	Up to 21		

3 PROJECT OPERATION

3.1 Test Strip

The paving of the test strip was initiated at 1 pm on October 24th, 2018 in Scott County, Missouri. Figure 1 shows the location of the project. Figures 2 and 3 show the paving process implemented using a concrete slip-form paving equipment. As indicated in Figure 3, the surface alignment was tested constantly, and the paver was adjusted accordingly.



Figure 1. Project location: 587 State Hwy PP Scott City, MO 63780



Figure 2. Paving process



Figure 3. Surface adjustments

The density test was conducted with a non-destructive method Nuclear Density Meter Ground Test Equipment at both sides of the pavement. Nuclear density gauge measures in-place density using gamma radiation. Gamma rays are emitted from the source and interact with electrons in the pavement through absorption, Compton scattering, and the photoelectric effect. A Geiger-Mueller detector (situated in the gauge opposite from the handle) counts gamma rays that reach it from the source. Pavement density is then correlated to the number of gamma rays received by the detector (<http://www.troxlerlabs.com>).



Figure 4. Density measurement

The test results showed that the density was not uniformly distributed. For the test strip, adjustments were made using addition of concrete and further compaction, as shown in Figure 5.



Figure 5. Density adjustments

Even after the further compaction, visual observation of the cross section of the pavement (Figure 6) showed that the pavement was less dense at both ends, while the compaction was effective at the center. The cast CCP was poor in paste at some parts. Therefore adjustment in the mixture design were made accordingly.



Figure 6. Visual observation of the cross section

3.2 Instrumentation

The sensor installation and instrumentation, including sensors for strain measurements due to environment, dynamic load response, and joint opening with minimal disturbance to grade were carried out by MnDOT. Figure 7 shows the positioning of the various instrumentation of Cells 1, 2 and 3.



Figure 7. Instrumentation operation

The applied sensors and gauges are shown in Figure 8. A brief description of each sensor is given in Table 3. Figure 9 illustrates the instrumentation schematics that were used.



Thermocouple Tree



Joint Opening Block Out



Vibrating Wire Strain Gauges



Dynamic Strain Gauges

Figure 8. Sensors and gauges applied in Cell 1, 2 and 3

Table 3. Instrumented sensors in Cells 1, 2 and 3

Item	Sensor	Description
1	Thermocouple Tree	To measure frost depth, temperature gradients in pavement layers and temperature compensation for other instruments
2	Joint Opening Block Out	Placed within 1-inch PVC conduit, which is held within a joint opening block out that crosses the joint between the two panels for measurement of the displacement of the pavement joint.
3	Vibrating Wire Strain Gauges	Two gauges were placed in the longitudinal and transverse direction of the pavement to evaluate the effects of both directions for determining effects of applied loads to the pavement
4	Dynamic Strain Gauges	Two more dynamic strain gauges were placed near the edge of the pavement in the longitudinal direction to measure the edge deflection due to traffic loads.

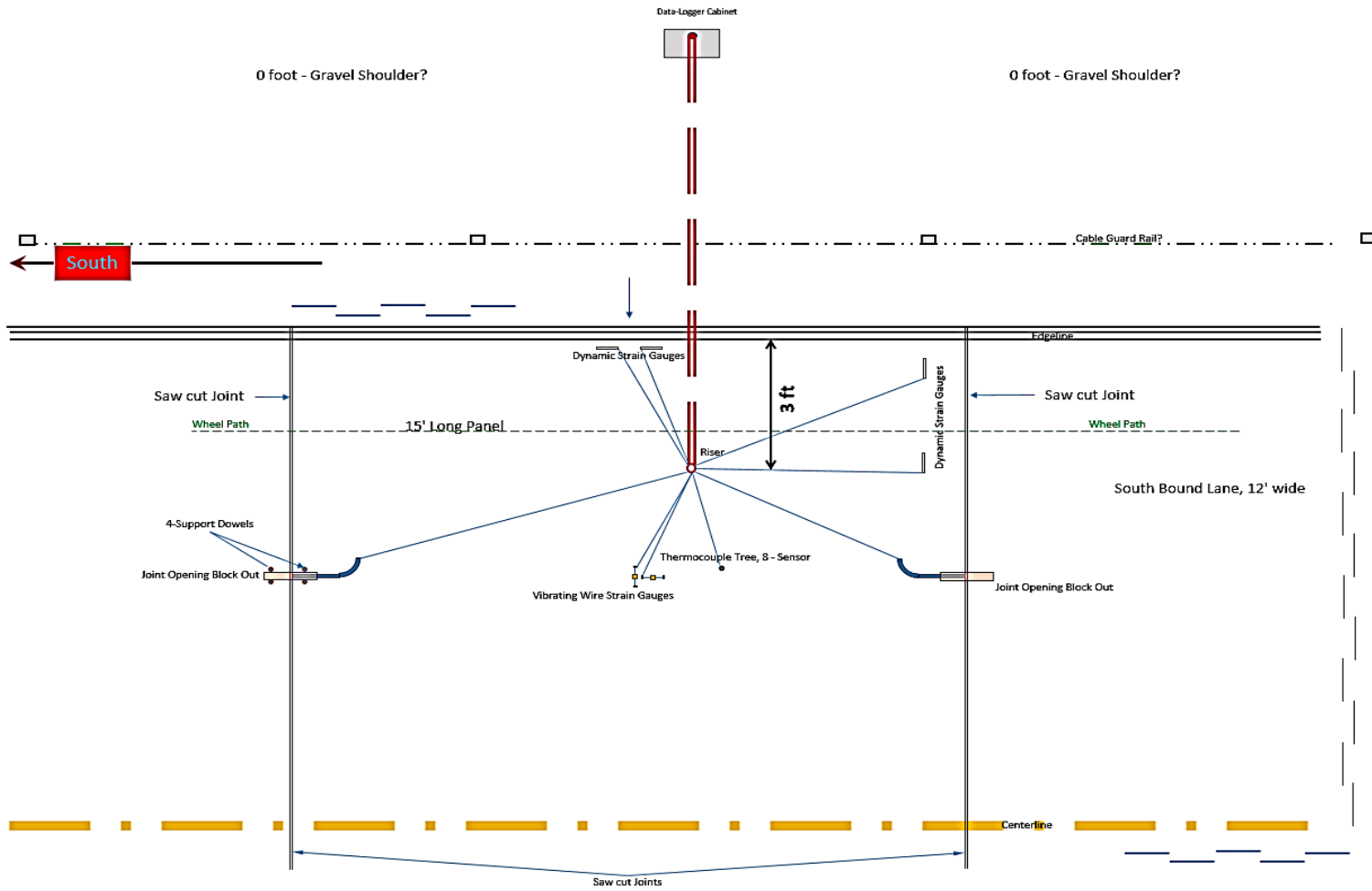


Figure 9. Instrumentation schematics (plan)

3.3 Paving Operations

Paving operations started at 12 pm on 25th of October 2018. The project was initially on hold due to precipitation. Figures 10 to 12 illustrate the phases associated with loading of the paver, compaction and measurements, and surface finishing. Curing in a form of spray was then applied, as shown in Figure 12.



Figure 10. Loading process of the slip-form paving



Figure 11. Paving and adjustments



Figure 12. Finishing process

3.4 Sampling

Cast-in-field samples were prepared at the plant site at I-55, Scott City, MO on October 25, 2018 (Figure 13). Two mixtures were sampled. A total of 18 prismatic molds measuring 6”×6”×24” were prepared to determine flexural properties, and 18 cylindrical molds measuring 6”×12” were cast to evaluate compressive strength. Mixture 1 represented Cells 1 and 2 as the base mixture without any fiber, while mixture 2 was reinforced with 5 pecy of synthetic fibers for Cell 3 casting. The moisture content of the CCP was maintained between 5% and 6% with the water-to-cementitious materials ratio (w/cm) ranging between 0.31 and 0.38. Figure 14 shows the sampling operation.



Figure 13. Location of the plant site: 800 Rose-Con Rd Scott City, MO 63780



Figure 14. Sampling of concrete

During sampling, the Vebe consistency time and density of the compacted concrete were measured, as per Procedure A of ASTM C 1170. The Vebe test setup is shown in Figure 15. The procedure is described in detail in Section 4.1.



Figure 15. Vebe test apparatus for determining consistency/density of fresh CCP

Compaction was adequately provided by a jackhammer using rectangular plates of measuring 5.75"×8" and circular plates measuring 5.75" in diameter. The concrete was cast in 3 and 4 layers for the prismatic and cylindrical molds, respectively (Figure 16). The compaction of cylindrical samples was carried out in compliance with ASTM C 1435.

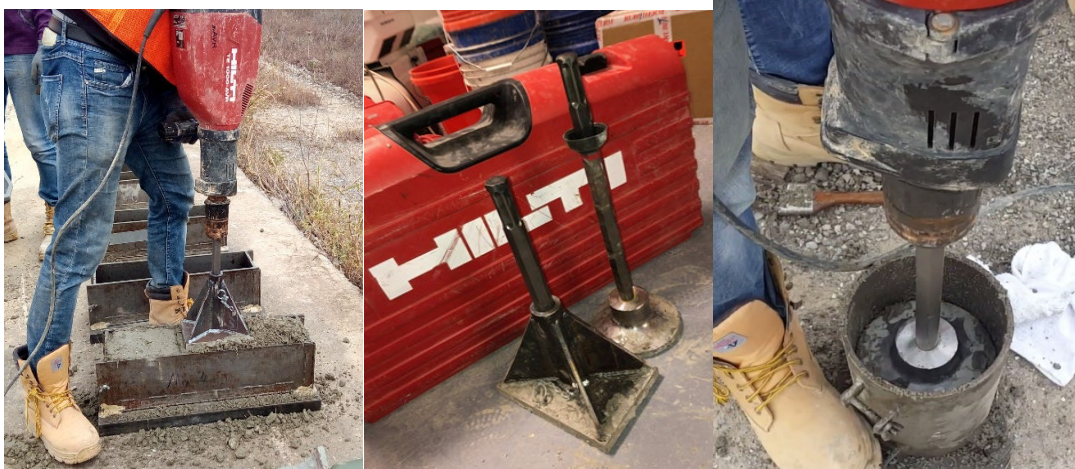


Figure 16. Compaction tools and process

The samples were covered with wet burlaps, followed by plastic sheets and blankets to maintain appropriate curing moisture and temperature. Figure 17 shows the samples after casting and prior to transport to the laboratory at Missouri S&T in Rolla, MO.



Figure 17. Sample curing and protection on site

On October 29th, the samples were demolded and transported to Missouri S&T. The transportation was done in compliance with ASTM C 31. Accordingly, the samples were protected with sand as suitable cushioning material in boxes to prevent damage from jarring. In order to prevent moisture loss during transportation, the samples were wrapped with wet burlap.

Transportation time was within 4 h, as allowed by ASTM. Figure 18 shows the demolding and transporting of the samples.



Figure 18. Demolding and transportation of samples

The samples were cured in standard curing conditions until the time of testing. The cylindrical samples were capped according to ASTM C 617 using high strength Sulphur capping compound (Figure 19). The cylinders were capped one day before compressive strength testing and were then returned to the moist curing room until the testing age. The samples were maintained in saturated conditions until the time of testing.



Figure 19. Demolding and transportation of samples

4 PROJECT OPERATION

This section reports the results from the various field and laboratory tests. The performance characteristics included fresh properties, mechanical properties (compressive and flexural strengths), drying shrinkage, and durability (freeze-thaw durability, 56-d rapid chloride ion permeability, bulk/surface electrical resistivity deicer salt scaling, and hardened air-void system). Throughout the report, Mixture 1 denotes the CCP mixture made without any fiber that was used for the construction of Cells 1 and 2, and Mixture 2 refers to the FRC employed for Cell 3.

4.1 Vebe Test (Consistency Time and Density)

The Vebe consistency time and density of fresh compacted concrete were measured during the paving in compliance with ASTM C 1170. The procedure consists of placing a representative sample of concrete of approximately 29.5 lb in a standardized cylindrical steel mold. The mold was fixed on a vibrating table, and a circular plastic plate was placed on top of the concrete sample. In order to consolidate the concrete, a removable mass of 50 lb was applied to the plate, and the vibrating table was turned on. Figure 20 shows the Vebe test apparatus for determining consistency/density of fresh CCP.

Table 4 summarizes the Vebe test results for mixtures 1 and 2. Based on the observation during the Vebe test of both mixtures, the mortar ring was not formed around the total perimeter of the surcharge within 60 s from the start of vibration. Therefore, the Vebe consistency time for both representative samples were reported to be greater than 60 s. Accordingly, both tested mixtures (with and without fibers) are categorized to have extremely dry consistency, as per

ASTM C1170. However, the test results showed that the incorporation of fibers increased the density of the fresh CCP by 15%.

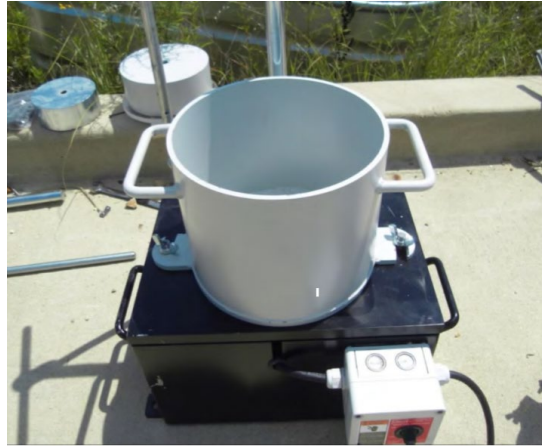


Figure 20. Vebe test

Table 4. Vebe test results

Mixture properties	Mixture 1 (No fiber)	Mixture 2 (with fiber)
Vebe consistency time (sec)	> 60	> 60
Density of fresh compacted concrete (lb/ft ³)	124	142

4.2 Compressive Strength

The compressive strength test was conducted in compliance with ASTM C39. The loading rate was maintained at 35 ± 7 psi/s. Table 5 shows the compressive strength results of cast-in-field Mixtures 1 and 2 at 7, 28, 91 days and saw-cut samples for Mixtures 1 and 2 at 91, 120, 180 days. The compressive strength of both Mixtures 1 and 2 increased with increase of curing time. For example, the increase of curing time from 7 to 91 d resulted in 104% and 20% higher compressive strength for cast-in-place Mixtures 1 and 2, respectively. The increase in curing time from 91 to 180 d resulted in 88% and 75% higher compressive strength of saw-cut Mixtures 1 and 2, respectively. The compressive strengths of cast-in-field samples were greater

than saw-cut samples. This can be related to the different compaction energy applied during sampling of the cast-in-field samples. For example, the 91-d compressive strength of the cast-in-field Mixtures 1 and 2 was 41% and 39% greater than that of cored specimens tested at the same age. The compressive strength of the FRC was greater than that of the concrete without fiber for both cast-in-field and saw-cut samples.

Table 5. Compressive strength of samples

	Mixture ID	Curing age (d)	Compressive strength 6”×12” cylinders (psi)				Coefficient of variation
			1	2	3	Average	
Cast-in-field sample	Mixture 1 (No fiber)	7	1650	1560	*	1605	3%
	Mixture 2 (5 pcy fiber)	7	4068	4370	*	4220	5%
	Mixture 1 (No fiber)	28	3726	3609	*	3667	2%
	Mixture 2 (5 pcy fiber)	28	5037	4874	*	4956	3%
	Mixture 1 (No fiber)	91	3268	3373	3186	3276	1%
	Mixture 2 (5 pcy fiber)	91	4424	5562	5198	5061	3%
Saw cut sample	Mixture 1 (No fiber)	91	1918	1806	2070	1931	4%
	Mixture 2 (5 pcy fiber)	91	3462	3461	2750	3103	5%
	Mixture 1 (No fiber)	120	2545	3185	*	2865	6%
	Mixture 2 (5 pcy fiber)	120	3720	3620	*	3670	2%
	Mixture 1 (No fiber)	180	3770	3510	*	3640	3%
	Mixture 2 (5 pcy fiber)	180	5625	4980	5700	5435	7%

Note: * denotes poorly consolidated samples

4.3 Flexural Strength Results

The flexural strength test was conducted on prismatic samples measuring 6”x6”x24” (span of 18”) according to ASTM C1609. The loading rate was maintained at displacement control of 0.0035 in./min until reaching a deflection of 0.02”. The rate of loading was then increased to 0.012 in./min until failure. Figure 21 shows the test set-up for the flexural test. The flexural strength was calculated as follows:

$$F = PL/bd^2 \quad (\text{Eq. 1})$$

where F is the strength (psi); P is the load (lbf); L is the span (in.); b is the average width of the sample (in.); d is the average depth of the sample (in.).



Figure 21. Flexural strength test

The residual strength was calculated by using the residual load in Eq. 1. The residual loads were determined at deflections of $L/600$ and $L/150$, respectively, according to Figure 22. The load-deflection results of the two tested cast-in-field Mixtures 1 and 2 at 7, 28, 91 days and the saw-cut samples for Mixtures 1 and 2 at 91, 120, 180 days are reported in Figure 23 and 24, respectively. The samples from Mixture 1 showed brittle failure behavior where failure occurred abruptly after reaching the peak load. The FRC mixture exhibited a sharp drop in load carrying capacity but maintained residual strength until a deflection of 0.12 in. Furthermore, the peak load of 91-d cast-in-place samples was greater than that of saw-cut specimens.

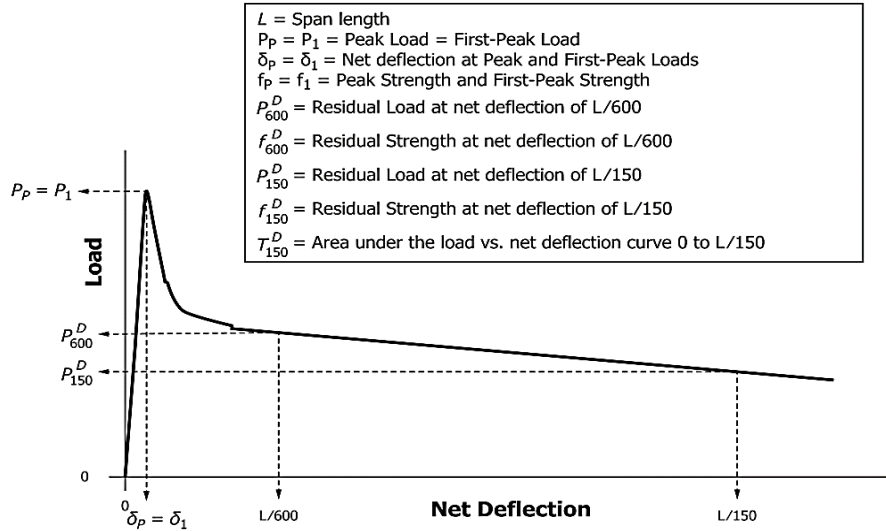


Figure 22. Example of parameter calculations for first-peak load equal to peak load

Table 6 summarizes the flexural strength and residual strength values for Mixtures 1 and 2 determined using cast-in-field samples at 7, 28, and 91 d as well as saw-cut samples that were tested at 91, 120, and 180 d. The flexural strength of both mixtures improved with curing time. The increase in curing time from 7 to 91 d resulted in 28% and 41% increase in flexural strength of cast-in-field samples for Mixtures 1 and 2, respectively. The increase in curing time from 91 to 180 d resulted in 45% and 41% increase in flexural strength of the saw-cut specimens for Mixtures 1 and 2, respectively. The incorporation of fibers slightly increased flexural strength of the cast-in-field samples, while the flexural strength slightly decreased for the saw-cut specimens. For example, the incorporation of fiber increased the flexural strength from 555 to 685 psi for the cast-in-place samples, while saw-cut specimens from FRC panels had a flexural strength of 295 psi compared to from 405 psi for non-FRC. Such considerable drop in in-situ flexural strength can be attributed to further complication in ensuring proper compaction in CCP made with fibers that had extremely dry consistency.

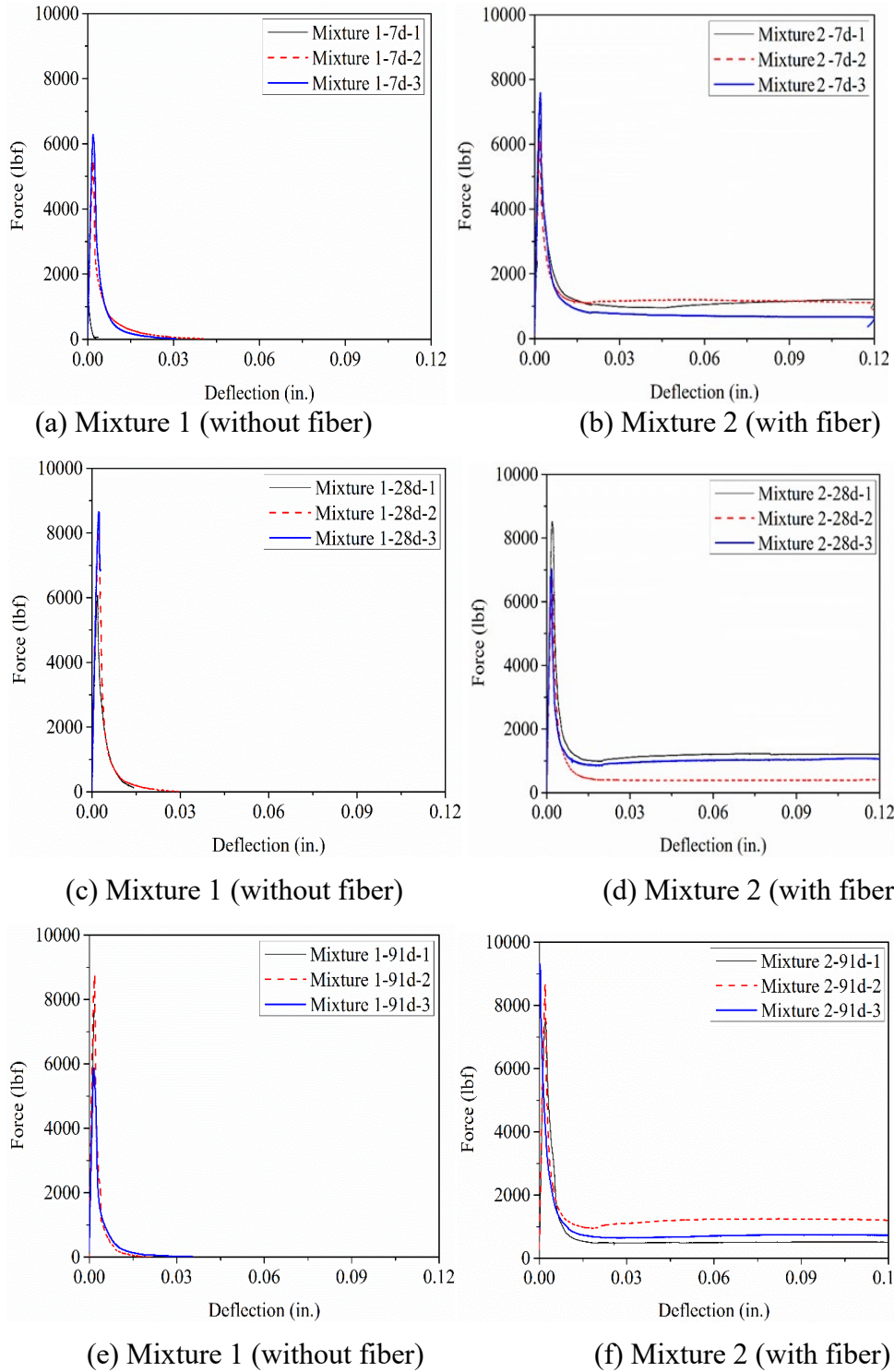
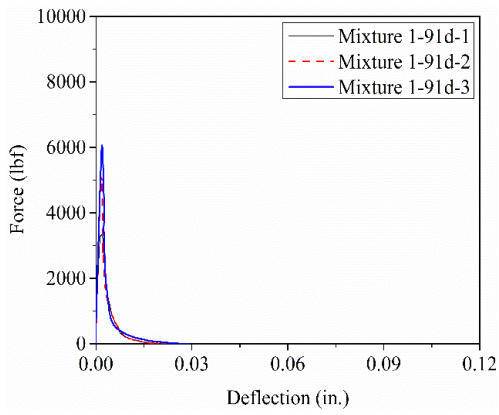
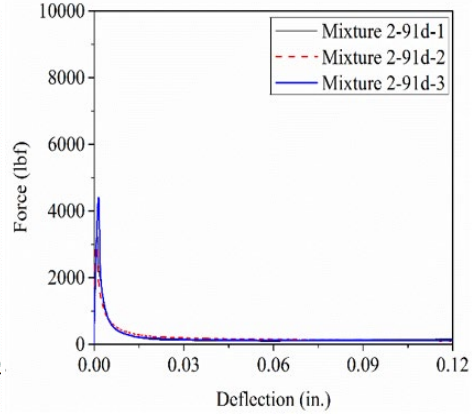


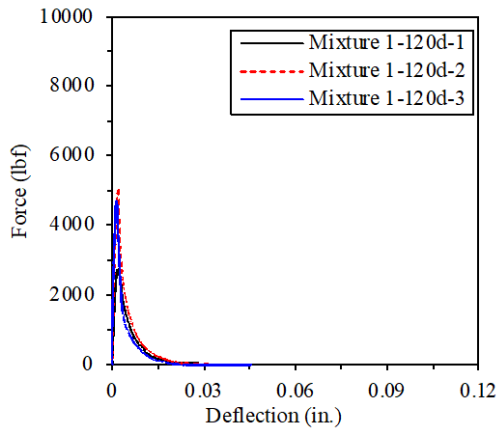
Figure 23. Load-deflection curves of three field-cast prismatic samples of the two investigated mixtures at 7, 28, and 91 days



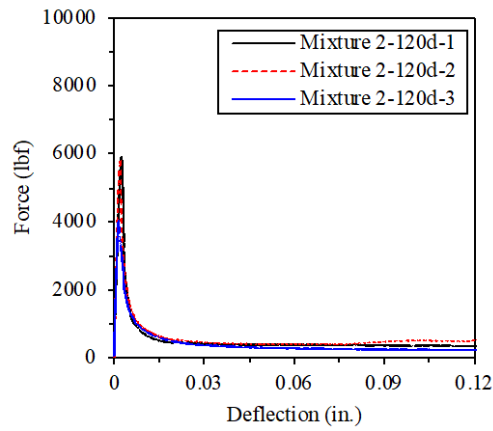
(a) Mixture 1 (without fiber)



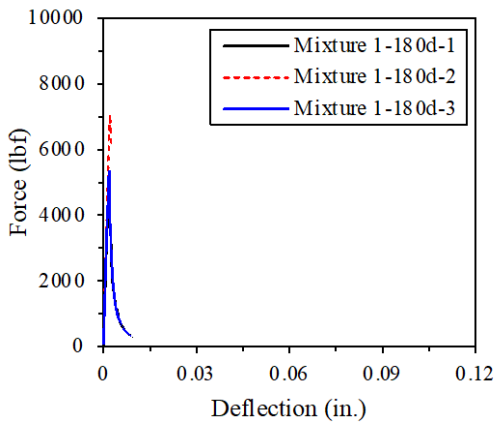
(b) Mixture 2 (with fiber)



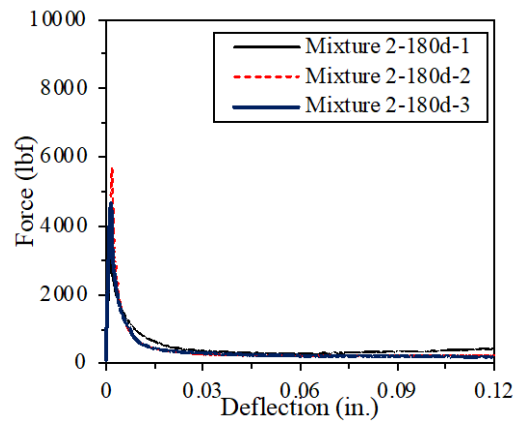
(c) Mixture 1 (without fiber)



(d) Mixture 2 (with fiber)



(e) Mixture 1 (without fiber)



(f) Mixture 2 (with fiber)

Figure 24. Load-deflection curves of three saw-cut prisms of the two investigated mixtures at 91, 120, and 180 days

Table 6. Flexural and residual strength results

Mix. ID	Flexural strength (psi)					Residual strength at deflection of L/600 (0.03") (psi)				Relative residual strength ratio (%)	Residual strength at a deflection of L/150 (0.12") (psi)				Relative residual strength ratio (%)
	1	2	3	Ave	COV (%)	1	2	3	Ave		Ave	1	2	3	
Mix. 1-7d (C)	402	483	419	435	10	0	0	0	0	0	0	0	0	0	0
Mix. 2-7d (C)	481	438	539	486	10	92	75	47	71	15	75	83	55	71	15
Mix. 1-28d (C)	466	616	664	582	18	0	0	0	0	0	0	0	0	0	0
Mix. 2-28d (C)	555	655	563	591	9	85	33	75	64	11	88	32	89	70	12
Mix 1 - 91d (C)	665	728	400	555	7	0	0	0	0	0	0	0	0	0	0
Mix 2 - 91d (C)	582	724	745	685	12	37	92	52	60	9	40	99	58	66	10
Mix 1 - 91d (S)	280	430	505	404	23	0	0	0	0	0	0	0	0	0	0
Mix 2 - 91d (S)	270	245	365	295	18	10	15	12	13	5	13	8	10	10	3
Mix 1-120 (S)	265	825	445	515	45	0	0	0	0	0	0	0	0	0	0
Mix 2-120 (S)	540	525	370	480	16	32	43	30	35	7	26	38	19	28	6
Mix 1-180 (S)	425	825	510	585	29	0	0	0	0	0	0	0	0	0	0
Mix 2-180 (S)	310	515	430	415	20	28	21	24	24	12	29	19	14	21	5

Note. C: cast-in-field samples; S: saw-cut samples; Ave: average; and COV: coefficient of variation.

4.4 Rapid Chloride Ion Permeability Test (RCPT)

The rapid chloride ion permeability of samples measuring 4"×2" was evaluated for saw-cut samples in accordance with ASTM C1202. Figure 25 shows the testing apparatus. The RCPT and test results are summarized in Tables 7 and 8. The results represent the average of three samples for each mixture. The RCPT values for Mixtures 1 and 2 were 3740 and 5090 Coulomb, respectively. This indicates that the Mixture 2 had relatively high electrical conductivity, while the Mixture 1 exhibited a moderate electrical conductivity. The higher RCPT value for Mixture 2 can be due to the higher porosity caused by the interfacial zone around the fibers as well as the lower compaction of the FRC.



Figure 25. Testing apparatus for RCPT

Table 7. RCPT scale for chlorides as per ASTM C1202

Passed charge	Permeability
> 4000	High
2000-4000	Moderate
1000-2000	Low
100-2000	Very low
< 100	Negligible

Table 8. RCPT results for saturated cores

Permeability	Charge passed (Coulomb)
Mixture 1 (without fibers)	3740
Mixture 2 (with fibers)	5090

4.5 Bulk/Surface Electrical Resistivity

Surface electrical resistivity of samples was measured in accordance with AASHTO T95. The surface resistivity test method consisted of measuring the resistivity of 4" × 6" cores using a four-point Wenner probe array, as illustrated in Figure 26. An AC potential difference was applied in the outer pins of the Wenner array generating current flow in the concrete. The potential difference generated by this current was measured using the two inner probes. The current used

and potential obtained along with the area affected were used to calculate the resistivity of cores. Bulk resistivity was also conducted on the same cored samples in compliance with ASTM C1760. In this method, bulk electrical resistivity was measured as the voltage between the two ends of cores as a small AC current was applied. The surface and bulk resistivity of concrete samples at the age of 91 days were measured for two samples of each mixture, and the average value is reported.

The surface and bulk resistivity values of the two investigated mixtures are shown in Tables 8 and 9 as $K\Omega.cm$, respectively. Mixtures 1 and 2 showed almost similar bulk resistivity values, which were 9.6 and 9.2, respectively. The surface resistivity was 52.8 and 44.1 $K\Omega.cm$, respectively. The results are conclusive that the inclusion of fiber to the mixture increased the electrical resistivity.



Figure 26. Testing apparatus for surface resistivity (left) and bulk resistivity (right)

Table 9. Bulk electrical resistivity of the two investigated mixtures ($K\Omega.cm$)

Mix ID	1	2	3	4	5	6	7	Ave.	Ave.
Mix 1-1	8.2	8.3	7.6	11.1	13	12.3	10.7	10.2	9.6
Mix 1-2	10	10.7	10.6	10.1	7.9	7.2	7.5	9.1	
Mix 2-1	8.6	7.2	7.5	7.2	6.8	7.2	7.8	7.5	9.2
Mix 2-2	10.9	10.7	11	10.8	11.2	10	11.4	10.9	

Table 10. Surface electrical resistivity of two investigated mixtures ($K\Omega \cdot cm$)

Mixture ID	Measure 1	Measure 2	Measure 3	Ave.	Ave.
Mixture 1-1	53.8	49.7	55.2	52.9	52.8
Mixture 1-2	52.6	53.4	51.8	52.6	
Mixture 2-1	47.8	46.5	46.9	47.1	44.1
Mixture 2-2	42.9	38.5	41.7	41.0	

4.6 Air-Void System

Samples measuring 4"×1" cut from cores were prepared to determine the air-void system according to ASTM C 457. Two samples for each mixture were tested. The time required for the measurement of each sample was about 10 min on average. Figure 27 shows sample preparation for air-void system analysis. Each sample was tested four times, rotating the sample by 90° each time, and the average of the four results was calculated as the air-void system parameters for that sample. By this means, the variations in the results would be averaged out, and more reliable values would be obtained.



Figure 27. Sample preparation for air-void system analysis

Table 11 presents the air-void system parameters of the two investigated mixtures. Both CCP mixtures were not air entrained. The air-void analysis includes large irregular voids that correspond to entrapped air bubbles in the concrete that had an extremely dry consistency. The total air content of Mixtures 1 and 2 were 4.0% and 5.1%, respectively. The greater air-void content of the Mixture 2 agrees well with results of RCPT (Table 8).

Table 11. Air-void content and spacing factor of the two investigated mixtures

Property	Mixture 1 (without fibers)	Mixture 2 (with fibers)
Air Content (%)	4.0	5.1
Paste to Air Ratio	6.25	5.52

4.7 Freeze-Thaw Resistance

The freeze-thaw resistance of saw-cut samples was evaluated in accordance with ASTM C666, Procedure A. The test procedure consisted of subjecting concrete samples to 300 cycles of rapid freezing and thawing in water at temperatures varying between 41 to -0.4 °F. For each mixture, three samples were tested, and the average was used to interpret the results. The samples were placed in metal containers and surrounded by approximately 0.2 in. of clean water in a specified chamber. Freezing was generated with a cooling plate at the bottom of the apparatus, whereas thawing was produced by heating elements placed between the containers. The dynamic modulus of elasticity of samples subjected to freeze-thaw cycles was determined to evaluate the extent of internal cracking due to frost damage.

Figure 28 shows the variations of dynamic modulus of elasticity during 220 cycles of saw-cut samples taken from the fiber-reinforced and non fiber-reinforced concrete pavements. For each concrete type, three samples were extracted from various locations in the pavement. Test results showed that the relative dynamic modulus gradually decreased for Mixtures 1 and 2

with the increase of freeze-thaw cycles. For each concrete type, the changes in dynamic modulus of elasticity were significantly different. This can reflect the uneven degree of consolidation of the concrete.

The durability coefficient was calculated as the square of the ratio of pulse velocities of P waves in the concrete at the end of the testing period to the value recorded at the beginning of the test, multiplied by the number of cycles at the termination of the test divided by 300. The test was terminated soon after the relative dynamic modulus of elasticity decreased to a level lower than 60%. Test results showed that the incorporation of fibers did not have a significant effect on frost durability. The relative dynamic modulus of elasticity at 220 cycles was 56% for Mixture 2, which translates into a durability coefficient of 41%. These values were 53% and 39% for Mixture 1, respectively. This indicates relatively poor frost durability of the CCP mixtures.

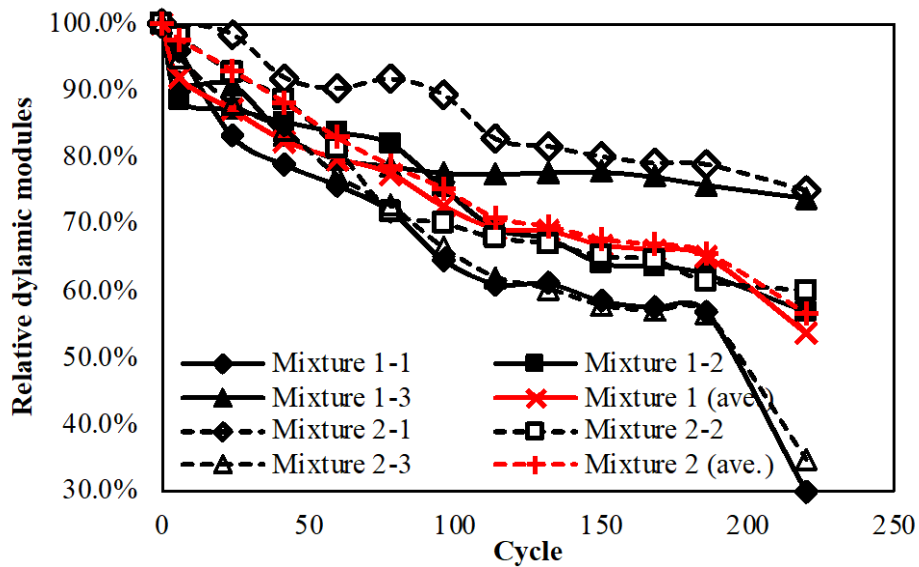


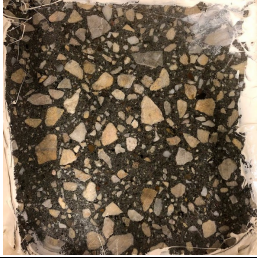
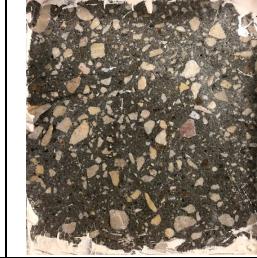
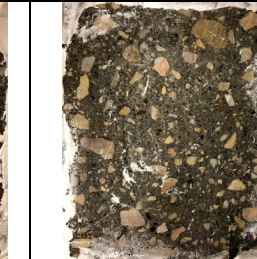
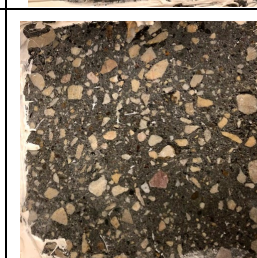
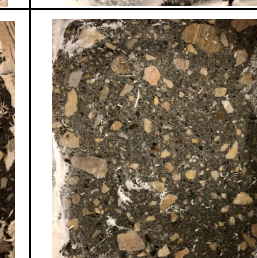
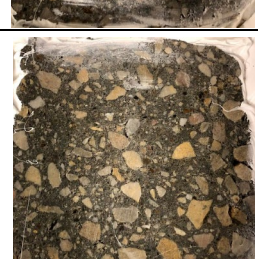
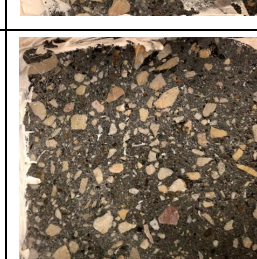
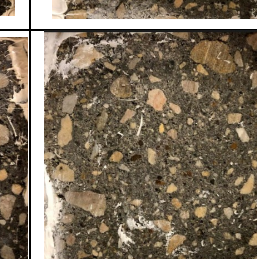
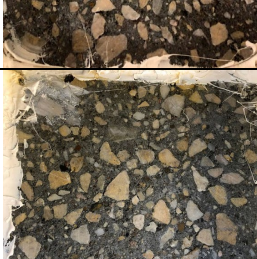
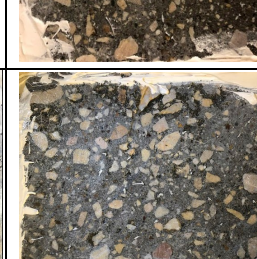
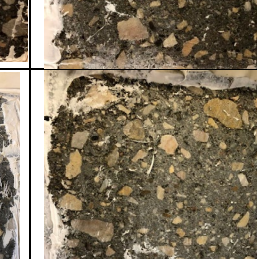
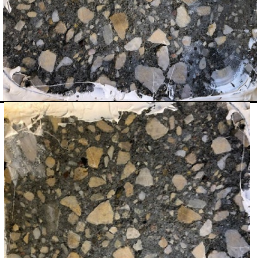
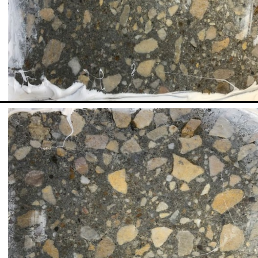
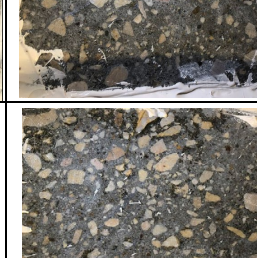
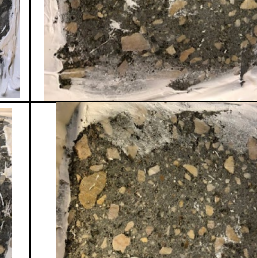
Figure 28. Variations of relative dynamic modulus of elasticity of Mixture 1 (without fibers) and Mixture 2 (with fibers) determined on saw-cut samples

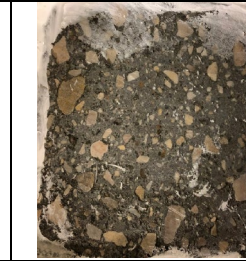
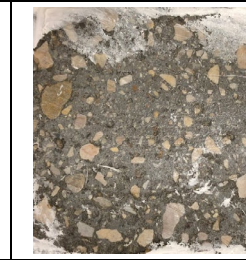
4.8 Deicing Salt-Scaling Resistance

Deicing salt scaling test was carried out using three saw-cut slabs measuring 11"×10"×3" for Mixtures 1 and 2 in accordance with ASTM C672. The test was conducted on two samples representing each mixture at the age of 91 days. During this test, the surface of the concrete was covered with approximately ¼ in. of 4% sodium chloride solution (0.14 oz. of NaCl for each 3.4 fl. oz. of water). The samples were subjected to 80 freezing and thawing cycles by alternately placing them in a freezing environment (-0.08 ± 3.02 °F) and a thawing environment (73.4 ± 3.1 °F). At the end of each series of five cycles, the salt solution was renewed, and the scaling residues were recuperated, dried, and weighed. The extent of surface scaling was assessed visually. The visual rating of zero means no scaling for concrete surfaces and five for severe scaling with coarse aggregates visible over the entire surface. The visual ratings of the concrete surface before testing and after 80 cycles of freeze-thaw shown in Table 12. No visible scaling was observed during 80 cycles indicating acceptable resistance of the mixture to salt scaling.

Table 12. Saw-cut slabs before and after exposure to salt scaling (80 cycles)

	Mixture 1-1	Mixture 1-2	Mixture 2-1	Mixture 2-2
Initial				
5 cycles				

10 cycles				
15 cycles				
20 cycles				
25 cycles				
35 cycles				
40 cycles				

45 cycles				
50 cycles				
55 cycles				
60 cycles				
65 cycles				
70 cycles				

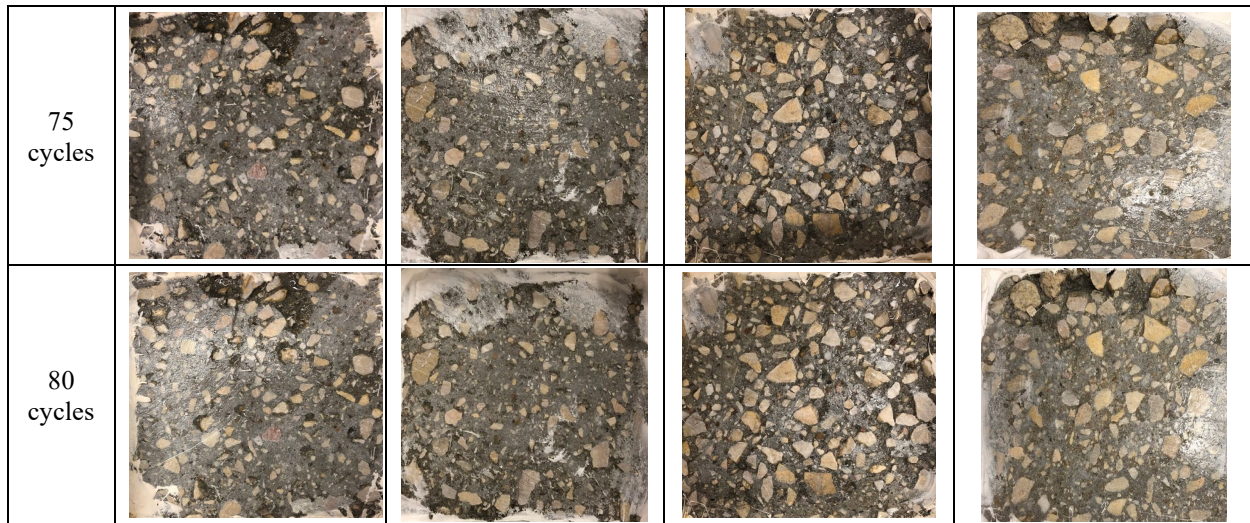


Figure 29 shows the variation of cumulative mass loss of the two mixtures during 80 test cycles. The cumulative mass loss increased rapidly with the increase of freeze-thaw cycles. The mass loss of Mixture 1 was noticeably higher than that of Mixture 2, especially after 35 cycles, where mass loss was around 0.17 lb/ft² (840 g/m²) compared to 0.10 lb/ft² (500 g/m²) for the FRC. However, the weight loss recorded for both mixture (with and without fibers) was below the acceptable range of 0.20 lb/ft² (1000 g/m²) at 50 cycles. This relatively good performance of the non-air entrained concrete is mainly attributed to the high surface density of the mixtures imparted by compaction during paving.

4.9 Drying Shrinkage

Drying shrinkage of mixtures was determined for saw-cut prisms measuring 3"× 3"×11.3" according to ASTM C157 using a digital type extensometer (DEMEC gauge). Shrinkage of saw-cut prisms were stored at 70 ± 3 °F and relative humidity of 50% ± 4% for the test period of 180 days. Figure 30 shows the shrinkage setup used and mass loss measurement. Figure 31 shows the variations of drying shrinkage of the two investigated mixtures over 180 days.

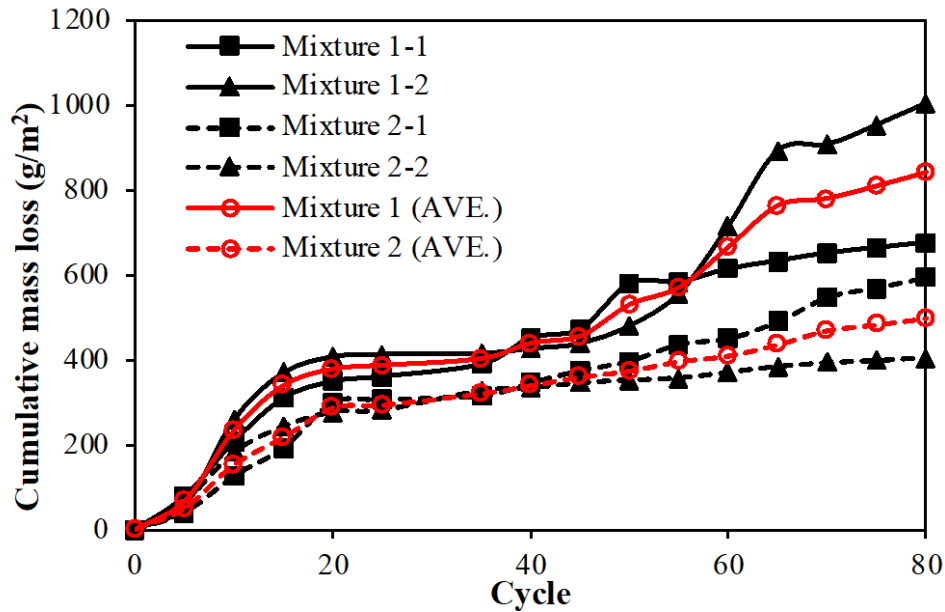


Figure 29. Variations of salt scaling mass loss of Mixture 1 (without fibers) and Mixture 2 (with fibers) determined on saw-cut samples



(a) Drying shrinkage testing



(b) Mass loss testing

Figure 30. Drying shrinkage and mass loss measurement

The concrete made without fibers had a large spread of shrinkage performance, as indicated in Figure 32 (a). This may be due to large variation in consolidation among the three saw cut samples or due to movement in the DEMEC point that was glued to the sample shortly before the beginning of testing. By ignoring the lowest shrinkage sample, the average of the two remaining samples would be similar to those of the fiber-reinforced CCP. The incorporation of

5 pcy of synthetic fibers led to less shrinkage, and all three samples had similar performance. The non-fibrous mixture had drying shrinkage of 1125 $\mu\epsilon$ when all three test samples were considered compared to 900 $\mu\epsilon$ in the case of the FRC.

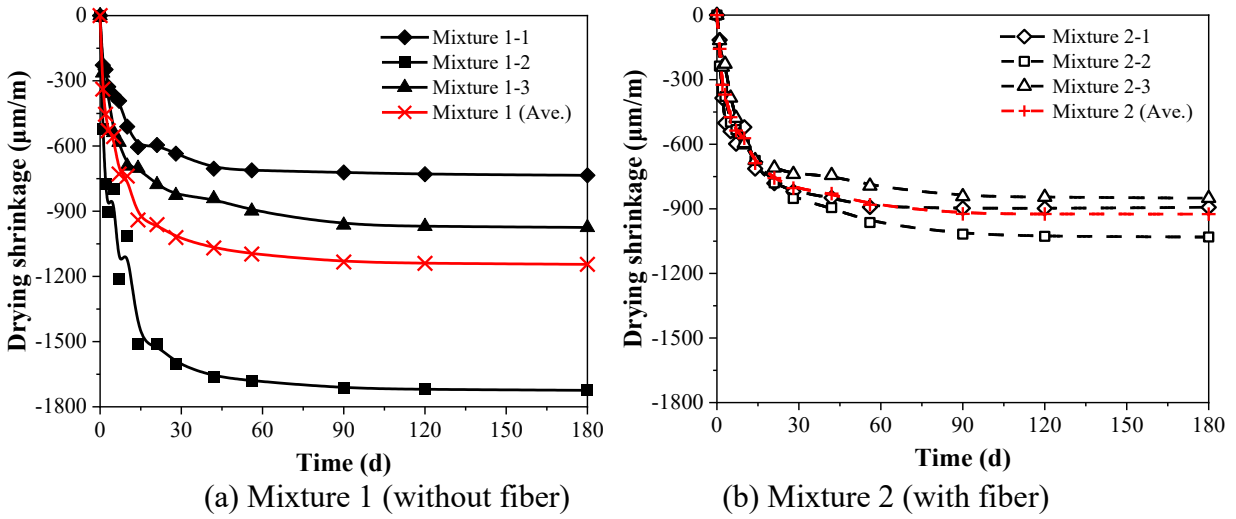


Figure 31. Variations of drying shrinkage determined on saw-cut samples

5 CELL PERFORMANCE

5.1 Curling and Warping

The curling and warping measurements were conducted as per ASTM E1364 on December 19th, 2018, September 27th, 2019, and September 16th, 2020. The measurements were conducted in the longitudinal, transverse, and diagonal directions (Figure 32). Both morning and afternoon measurements were taken on the day of testing to obtain values under variable temperature and moisture conditions. The last curling and warping measurement made on September 16th were conducted in the morning due to consistent temperature and humidity throughout the day.

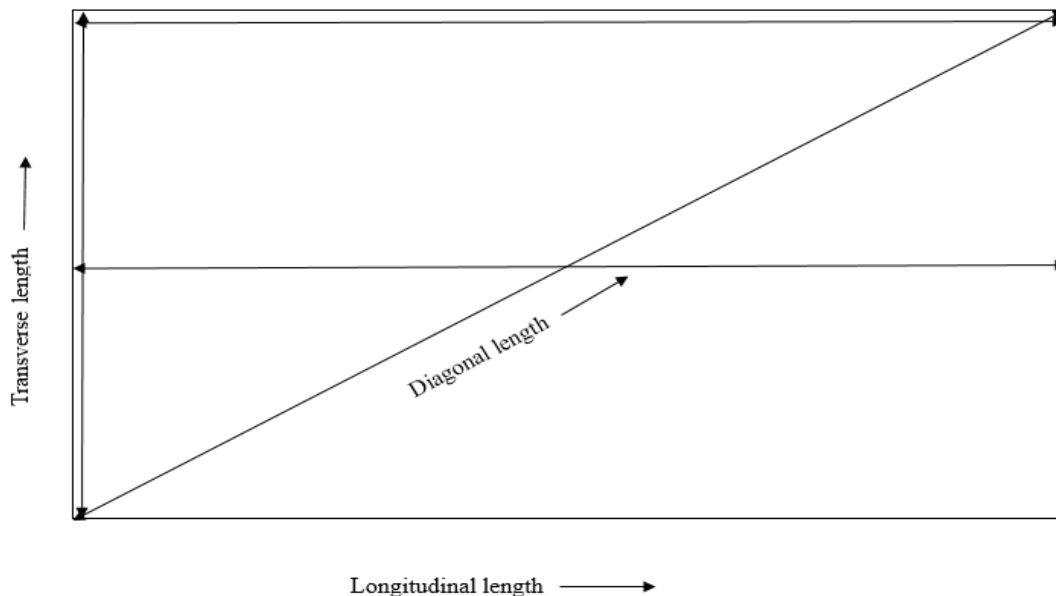


Figure 32. Direction of measurements - longitudinal, diagonal, and transverse lengths

Figure 33 shows the testing equipment comprised of two steel columns (A and B) connected with metal string adjusted and tightened with roller components of the columns. The test was developed by Iowa State University. For precise measurement, columns A and B were

anchored at joints (discontinuities between two cells), as shown in Figure 34. Then, the string was hooked off from column A and drawn to pass through the roller in column B. The string was then tightened firmly by adjusting a handle in column B. Two pins were placed under the string to make it tightened to avoid formation of sagging of string. A measuring tape was spread out along the string to record the locations of measured points. Prior to measurements, the pavement surface was cleaned, and temperature and ambient relative humidity (RH) were recorded. The data are tabulated in Table 13.



Figure 33. Test setup and measuring equipment

Table 13. Temperature and relative humidity data

Date	Time	Temperature (°F)	Relative humidity (%)
12/19/18	Morning	49	66
	Afternoon	53	69
09/27/19	Morning	84	60
	Afternoon	88	53
09/16/2020	Morning (11:30 AM)	76	67

The measurement was conducted at a maximum measuring interval of 2 ft for Class 2 resolution (ASTM E1364). However, at critical locations of curling and warping (e.g., cell edges

and center), intervals of 2 in. measurements along the profile were taken. A digital height gauge was used as a measuring gauge considering its convenient operation in the field. The data were collected at eye level to the string.

Figures 34-36 compare the curling and warping readings of Cells 1 and 3 prepared without and with fibers, respectively, and both with panel lengths of 12 ft. Figure 37-39 compare curling and warping readings of Cells 1 and 2 both made without fibers with different panel sizes of 12 and 15 ft, respectively, using four reading directions (Figure 33). The results show that Cell 3 cast with FRC had more significant deflection, especially those recorded in the diagonal direction, than non-FRC of the same panel length. Deflection readings of Cell 3 ranged from -1.25 to 0.5 in. compared to -0.5 to 0.5 in. for Cells 1 and 2 cast with non-FRC. The increased deflection of Cell 3 can be related to higher crack resistance developed by the fiber reinforcement. Possible formation of microcracks in Cells 1 and 2 (without fibers) can increase the degree of freedom of the system and reduce the deformation. On the contrary, comparing the results from Cells 1 and 2 (Figure 37-39) showed that size of the cells had some influence on the curling and warping deflection.

Comparing the test results conducted on 12/19/18 and 09/16/20 indicate that the increase in elapsed time leads to a higher scatter in the deflection data. This is possibly due to the increase in the curling and warping in the cells with time. Additionally, no significant difference in the deflection can be observed between the fiber reinforced and non-fiber reinforced concrete cells of different lengths.

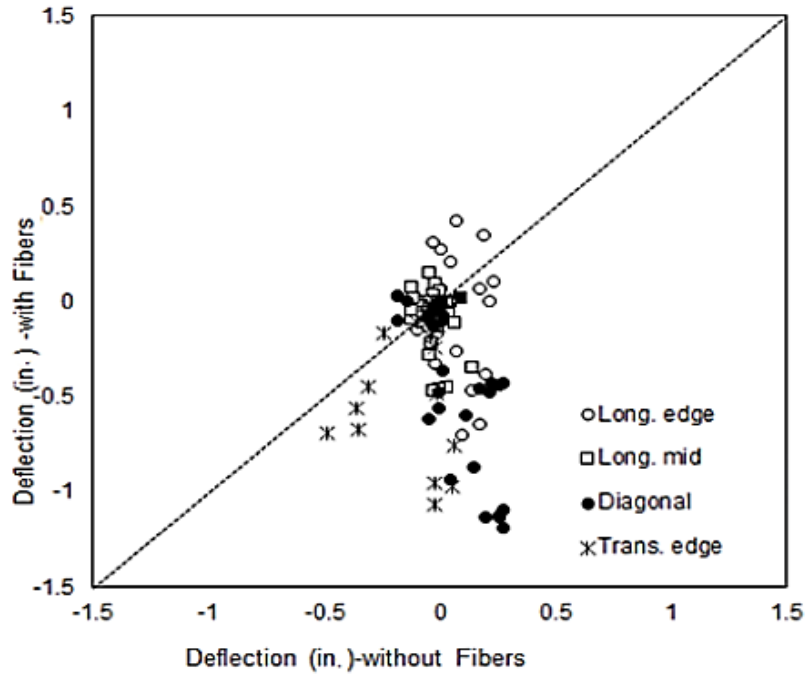


Figure 34. Deflection of cell 1 made without fibers vs. cell 3 made with fibers (L=12 ft) measured on 12/19/18

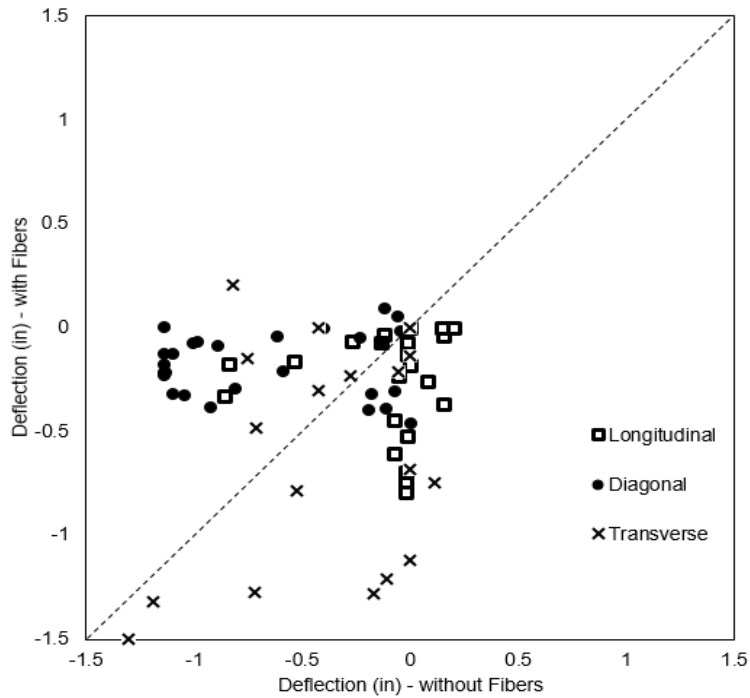


Figure 35. Deflection of cell 1 made without fibers vs. cell 3 made with fibers (L=12 ft) measured on 09/27/19

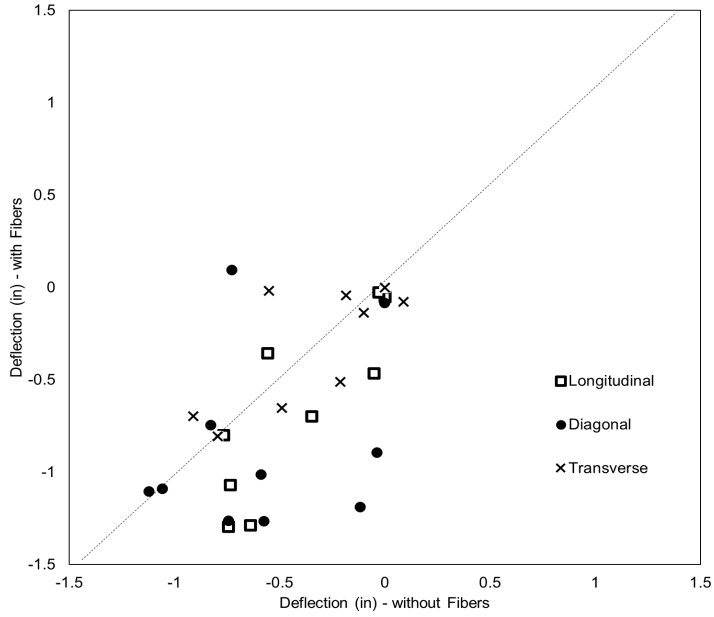


Figure 36. Deflection of cell 1 made without fibers vs. cell 3 made with fibers (L=12 ft) measured on 09/16/20

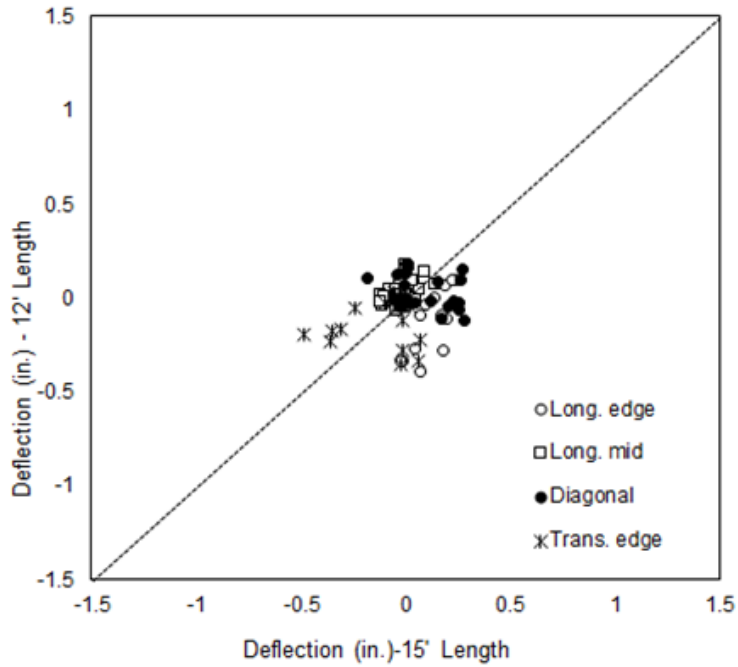


Figure 37. Deflection (in.) of cells without fibers with L=12' (Cell 1) vs. L=15' (Cell 2) - 12/19/18

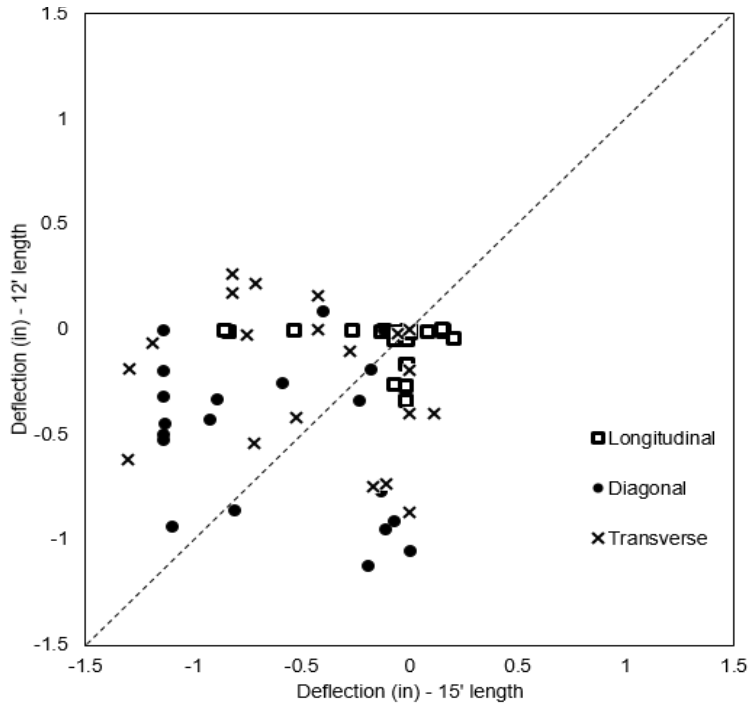


Figure 38. Deflection (in.) of cells without fibers with L=12' (Cell 1) vs. L=15' (Cell 2) - 09/27/19

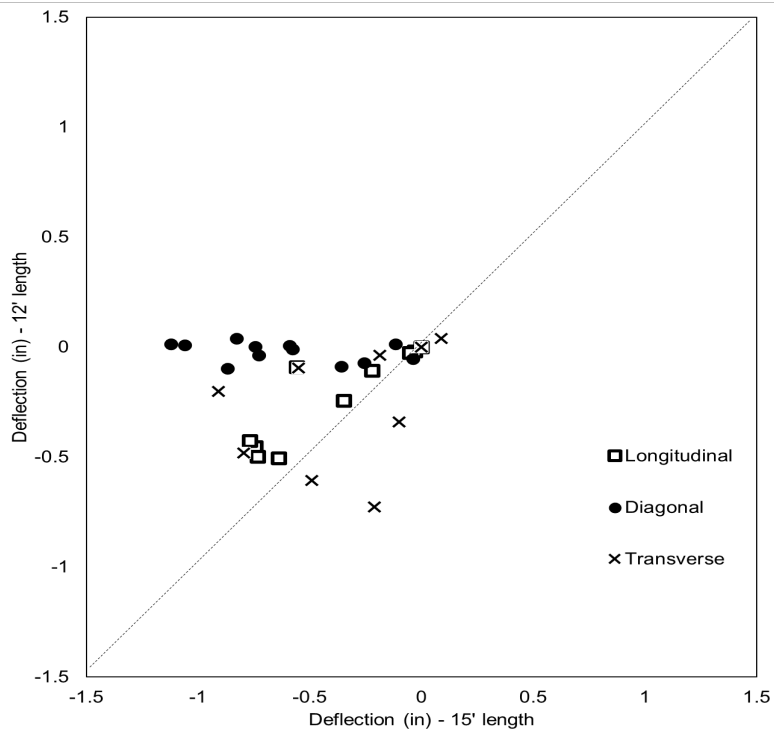


Figure 39. Deflection (in.) of cells without fibers with L=12' (Cell 1) vs. L=15' (Cell 2) - 09/16/20

5.2 Falling Weight Deflectometer

The falling weight deflectometer (FWD) was conducted on September 16th, 2020 by MoDOT. Figure 40 shows the equipment that was employed to measure the deformations and the schematic of the loading plate and transducer locations.

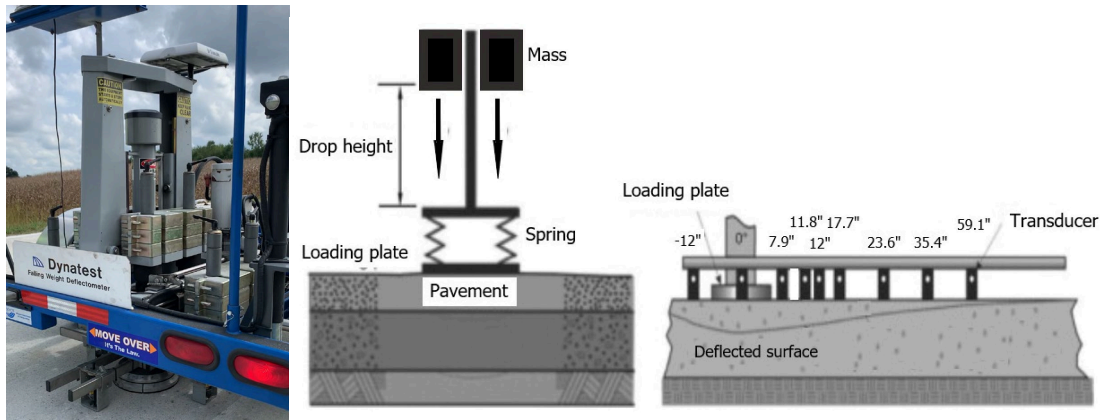


Figure 40. FWD equipment and schematic of loading plate and transducer location (drawing is adopted from Wang and Birken, 2014)

The analysis included the calculation of FWD deflection values as well as the load transfer efficiency (LTE) across joints derived from the readings of FWD at the three CCP slabs (Cell 1, Cell 2, and Cell 3). The deflection was measured using nine transducers with varying distances from the loading plate, as shown in Figure 40. The measurements were conducted under three loading rates of 80-81 psi, 107-109 psi, and 140-142 psi, respectively.

Figures 41-57 show the FWD deflection values for 14 joints, under three different stress levels for Cells 1, 2, and 3. The deflection values were inversely proportional to the distance from the loading point but directly proportional to the stress. It can be observed that the measured deflection followed a similar trend for all cells. The decreasing deflection condition from the loading plate to the furthest transducer shows that there was no crack or critical void in any of the tested slabs. However, the deflection values at Cell 3 made with FRC were higher than the other

two stations where concrete was prepared without any fibers. For example, at the highest stress of 140-142 psi, the deflection values at Cell 3 varied between 10.1-13 microns compared to 8.6-13 and 7.8-11.3 microns at Cell 2 and Cell 1, respectively. The deflection level is a function of the pavement structure and is influenced by the strength or stiffness of the layer and the support of the subgrade. Higher deflection of the Cell 3 can be due to the voids that were formed in the interfacial transition zone of fibers as well as the greater entrapped air in the stiff FRC. Another factor that can contribute to the higher deflection can be associated with a weaker subgrade support.

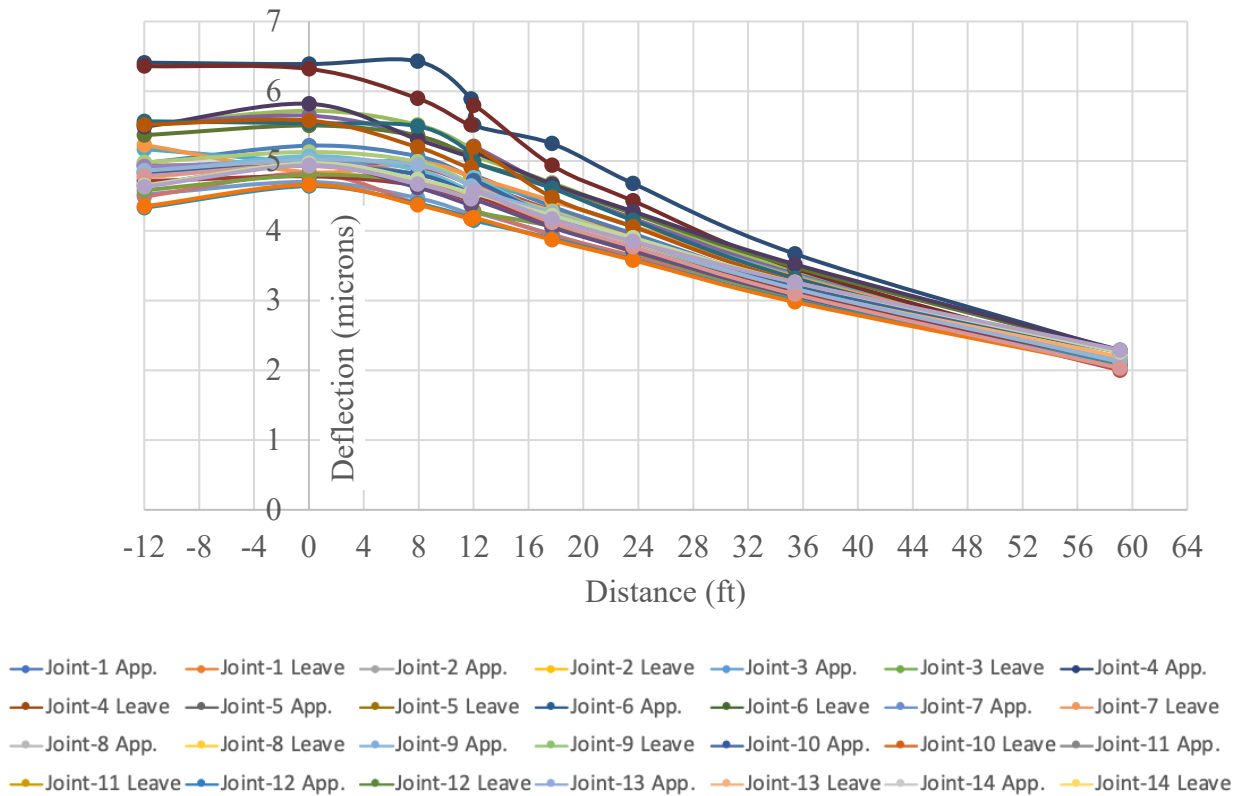


Figure 41. FWD Deflections at Cell 1 (Stress 80-81 psi)

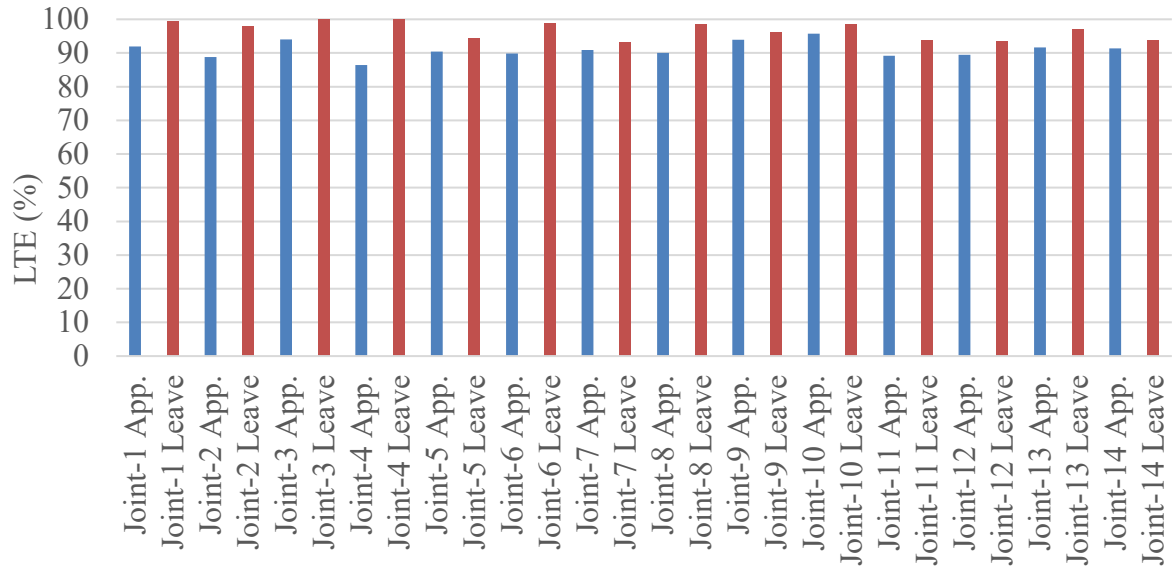


Figure 42. LTE (%) at Cell 1 (Stress 80-81 psi)

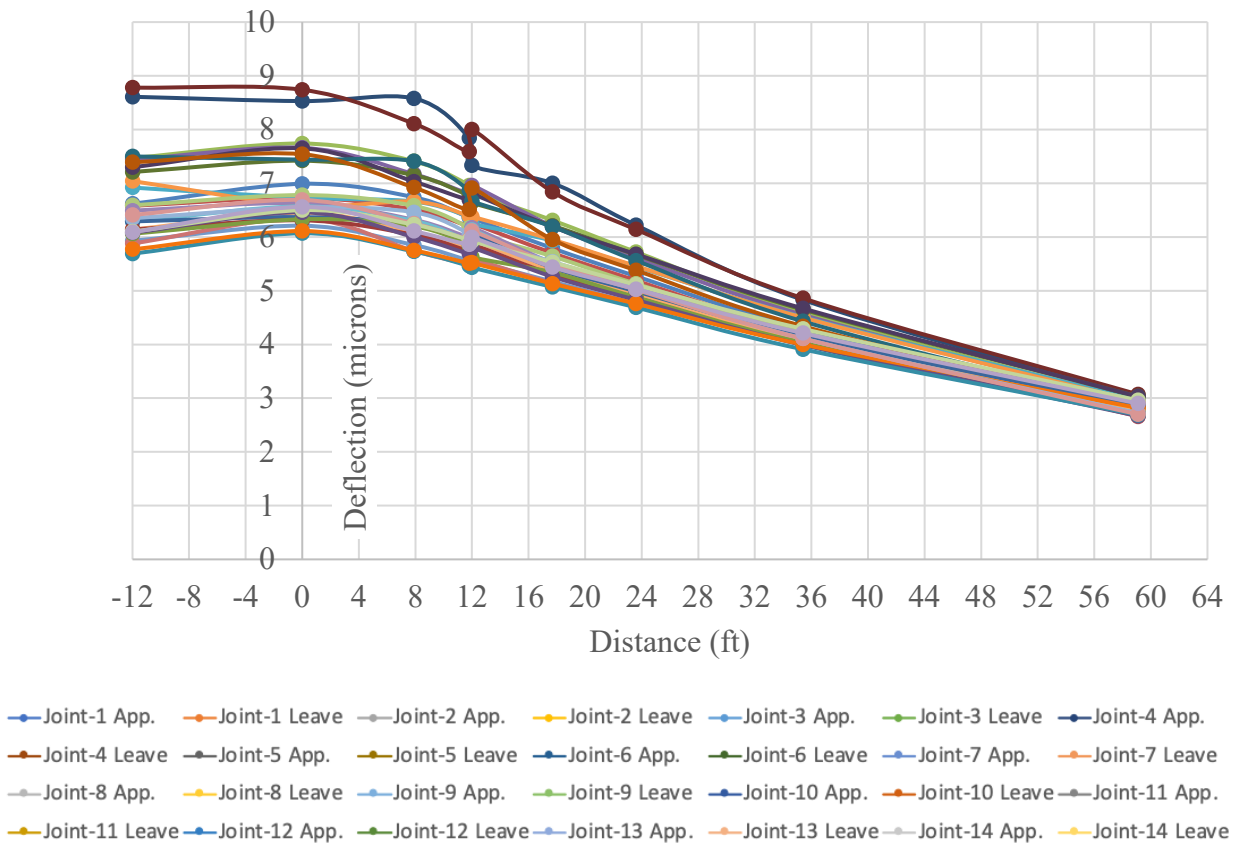


Figure 43. FWD Deflections at Cell 1 (Stress 107-109 psi)

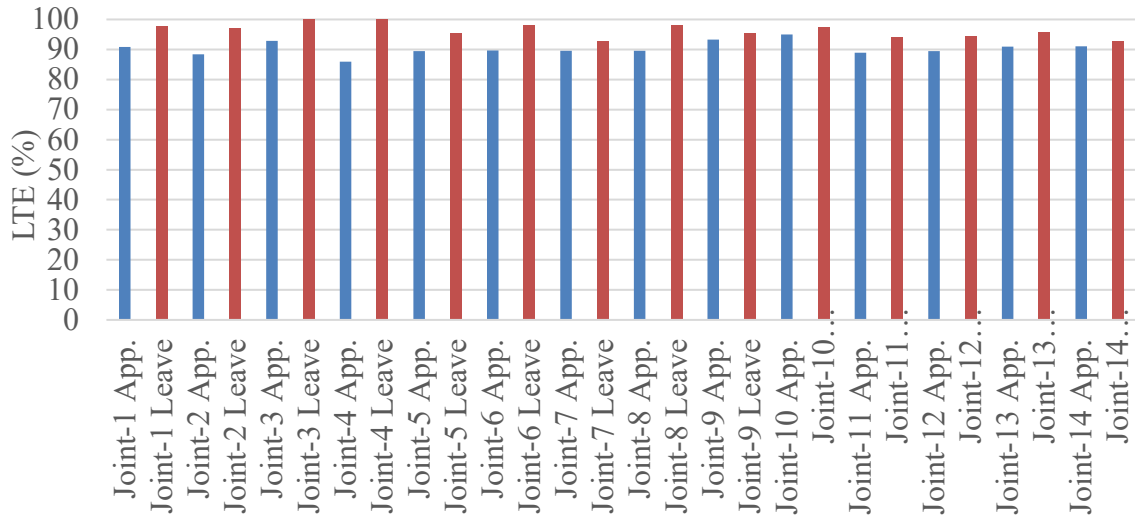


Figure 44. LTE (%) at Cell 1 (Stress 107-109 psi)

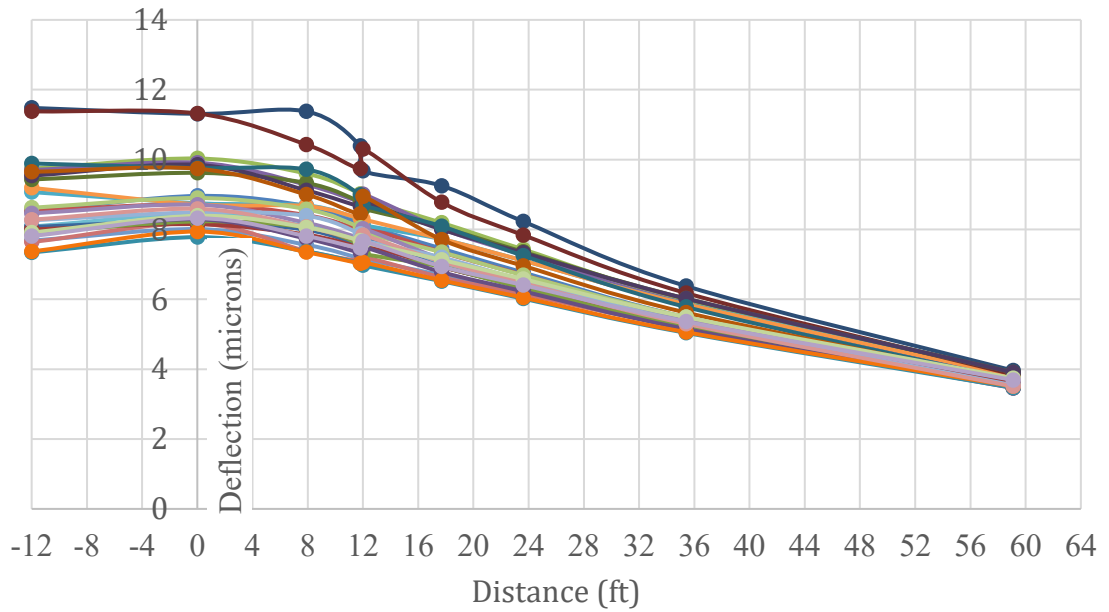


Figure 45. FWD Deflections at Cell 1 (Stress 140-142 psi)

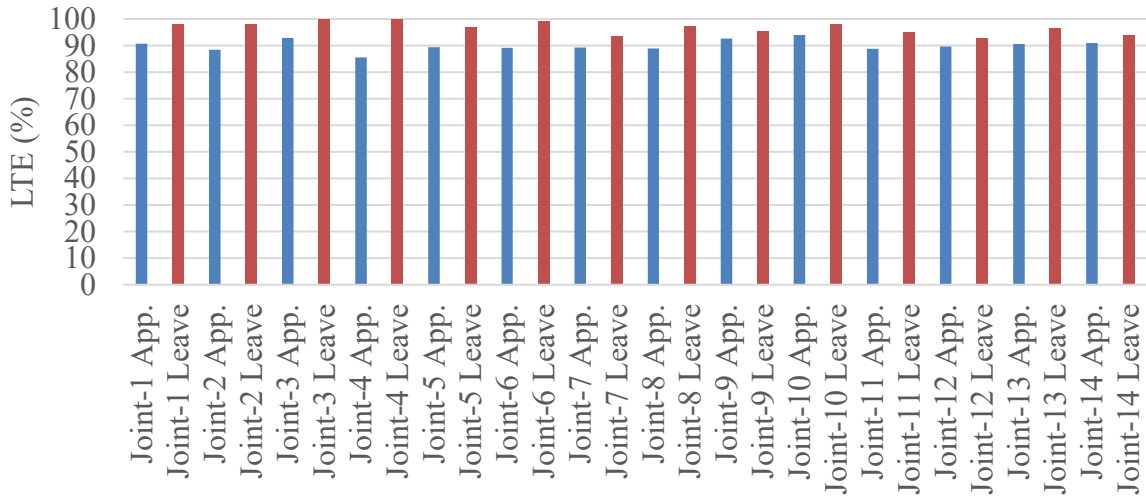


Figure 46. LTE (%) at Cell 1 (Stress 140-142 psi)

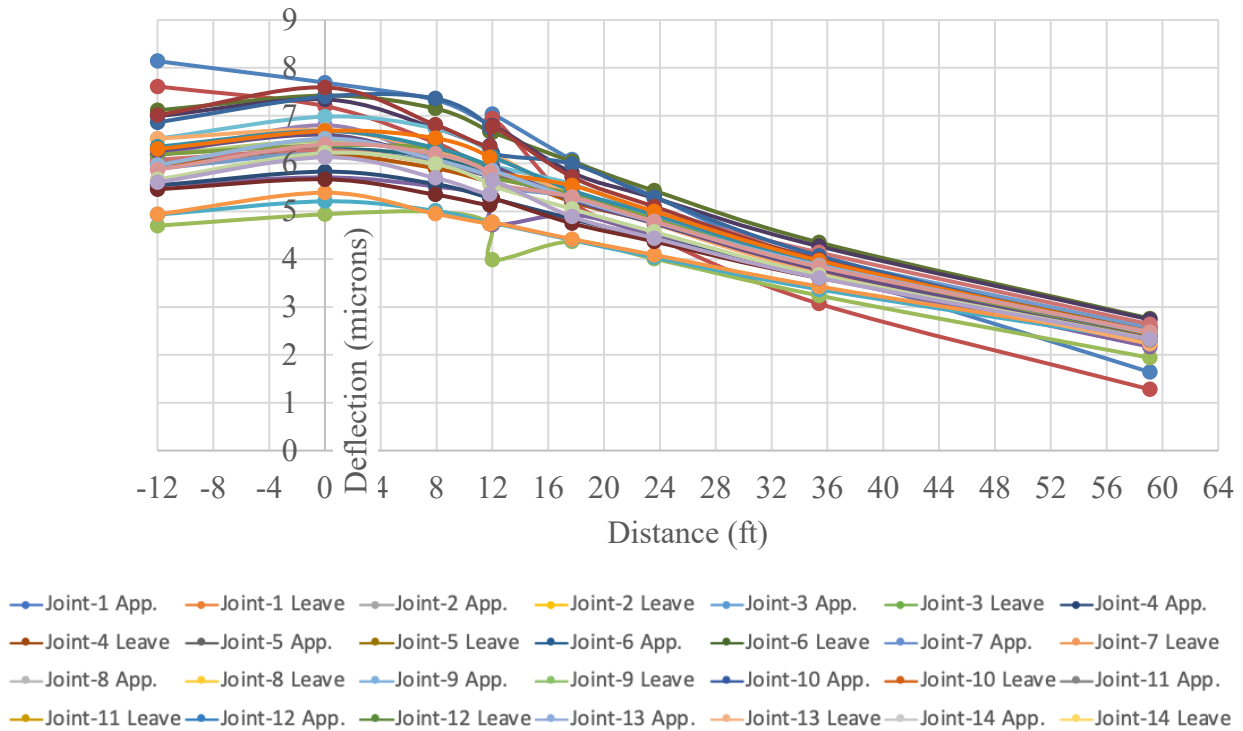


Figure 47. FWD Deflections at Cell 2 (Stress 80-81 psi)

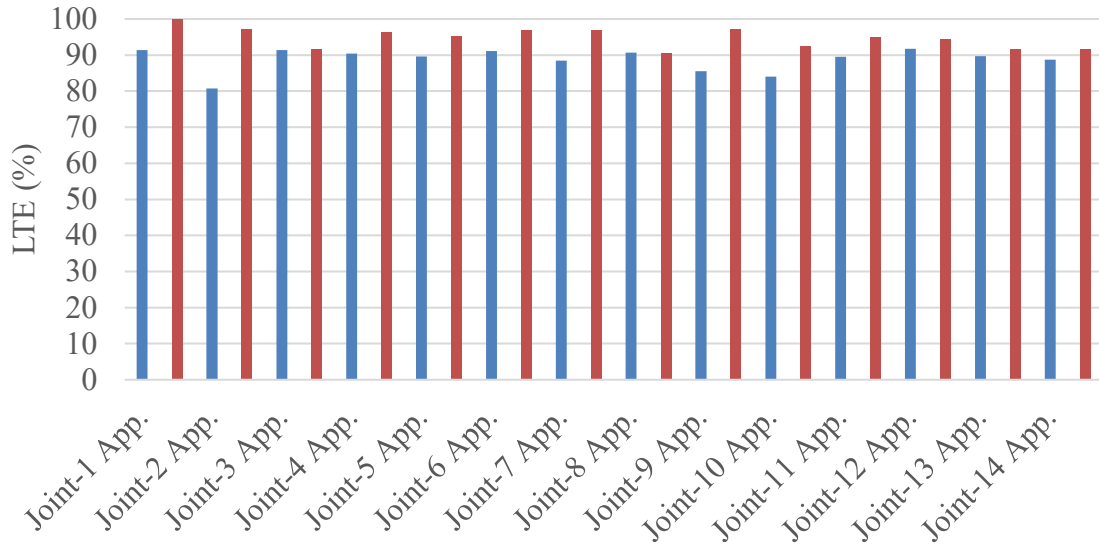


Figure 48. LTE (%) at Cell 2 (Stress 80-81 psi)

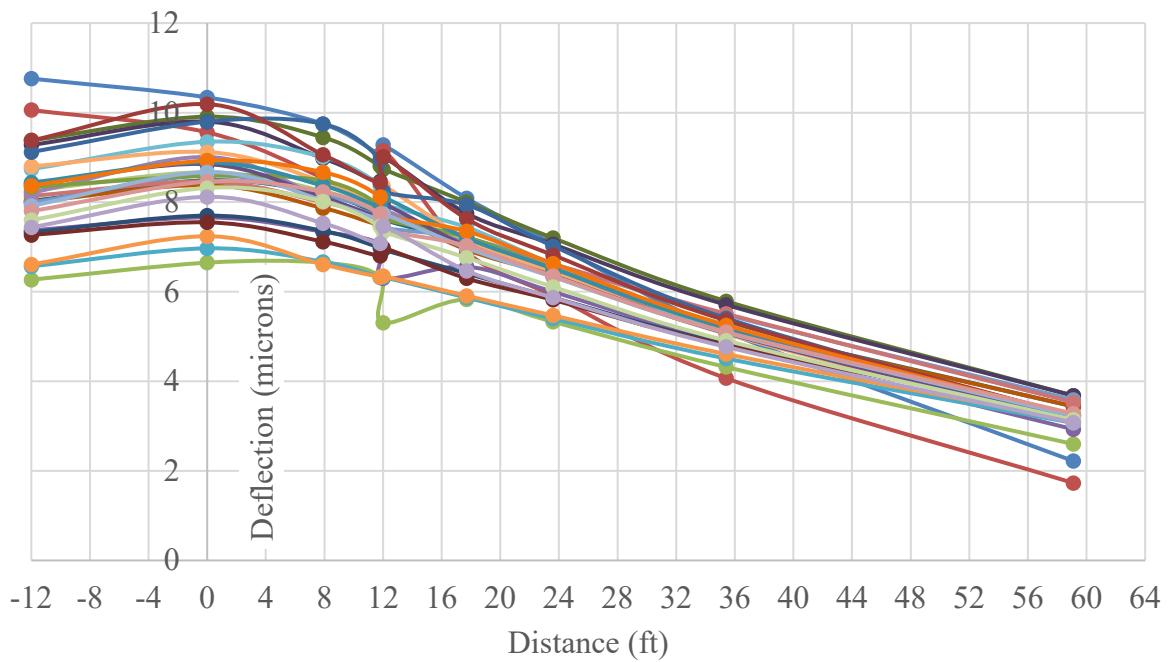


Figure 49. FWD Deflections at Cell 2 (Stress 107-109 psi)

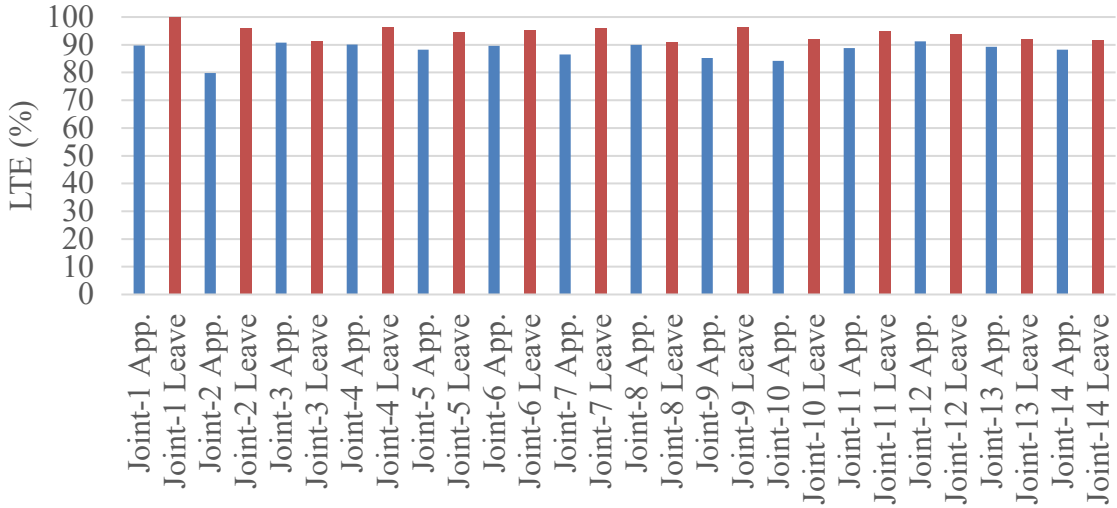


Figure 50. LTE (%) at Cell 2 (Stress 107-109 psi)

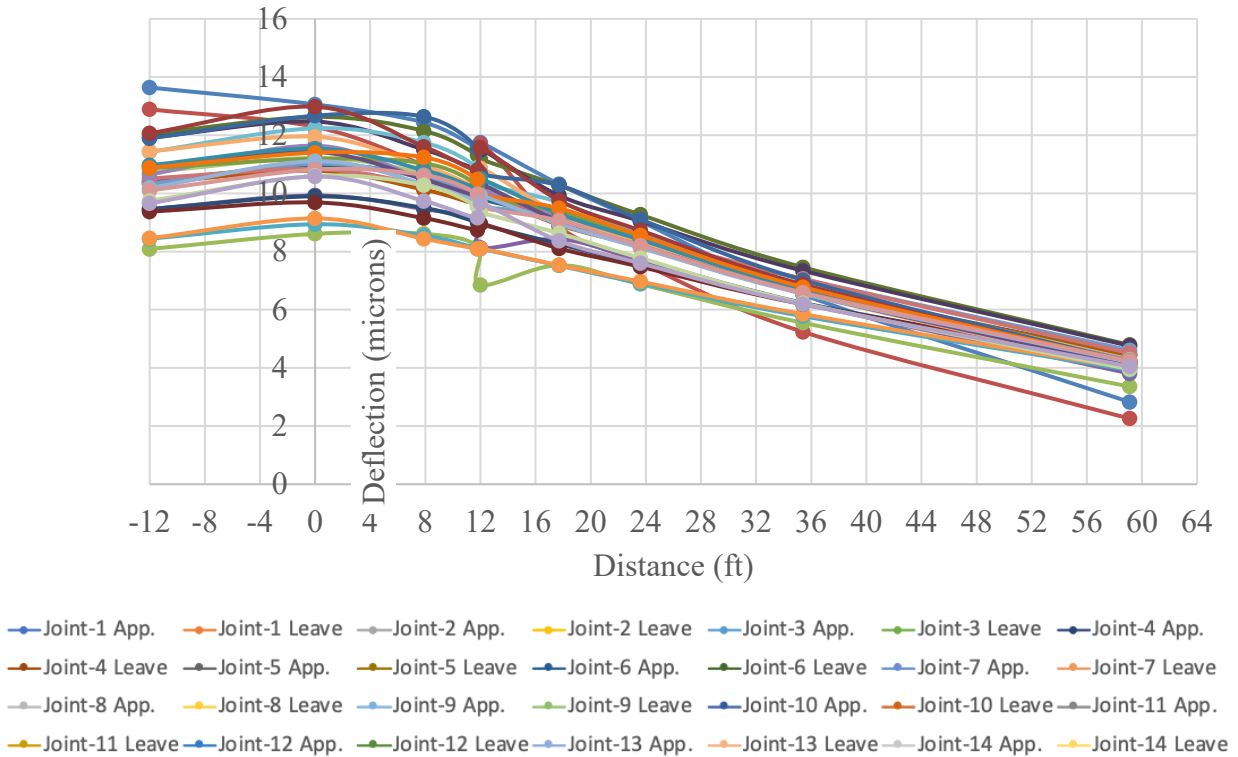


Figure 51. FWD Deflections at Cell 2 (Stress 140-142 psi)

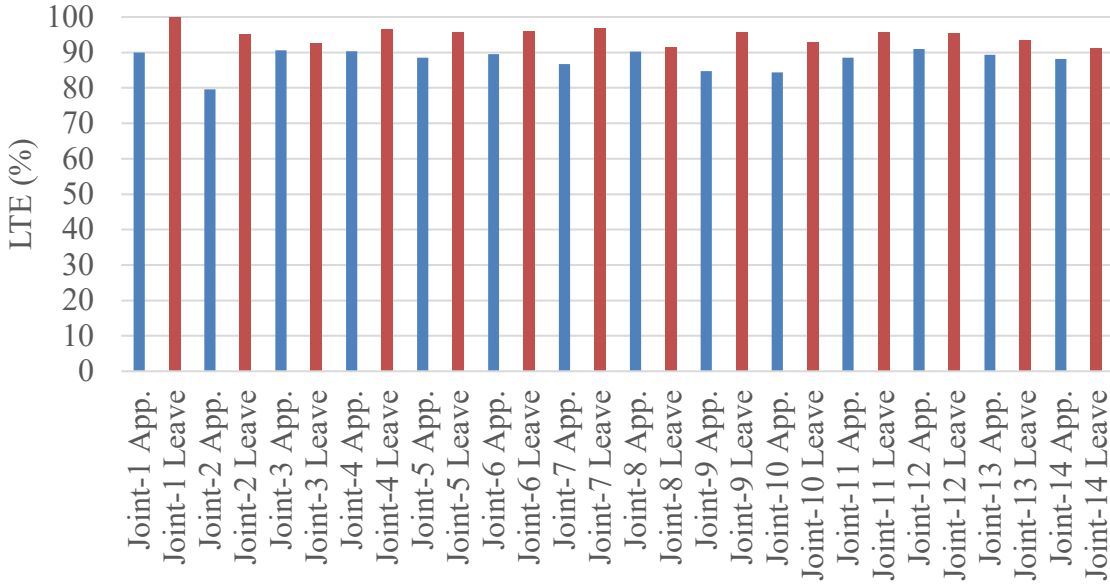


Figure 52. LTE (%) at Cell 2 (Stress 140-142 psi)

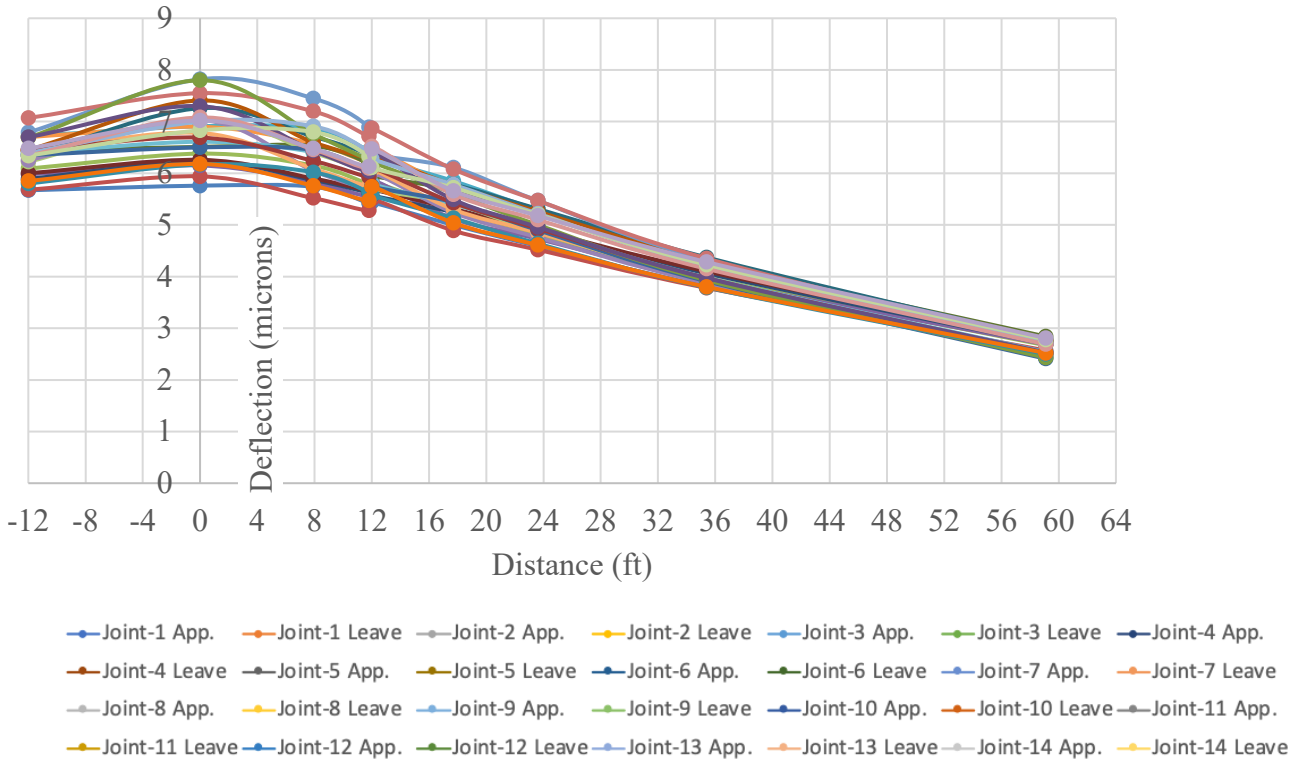


Figure 53. FWD Deflections at Cell 3 (Stress 80-81 psi)

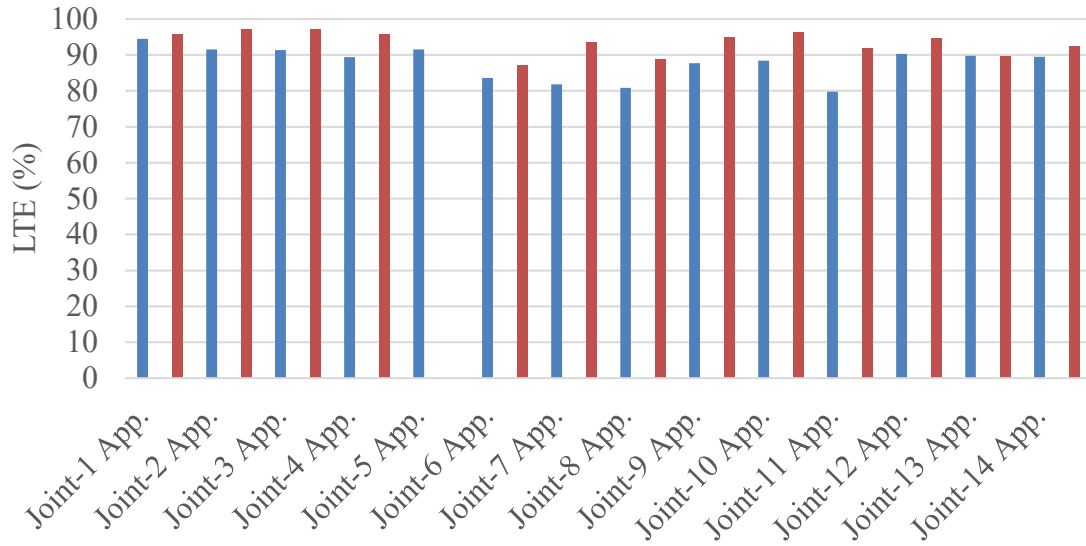
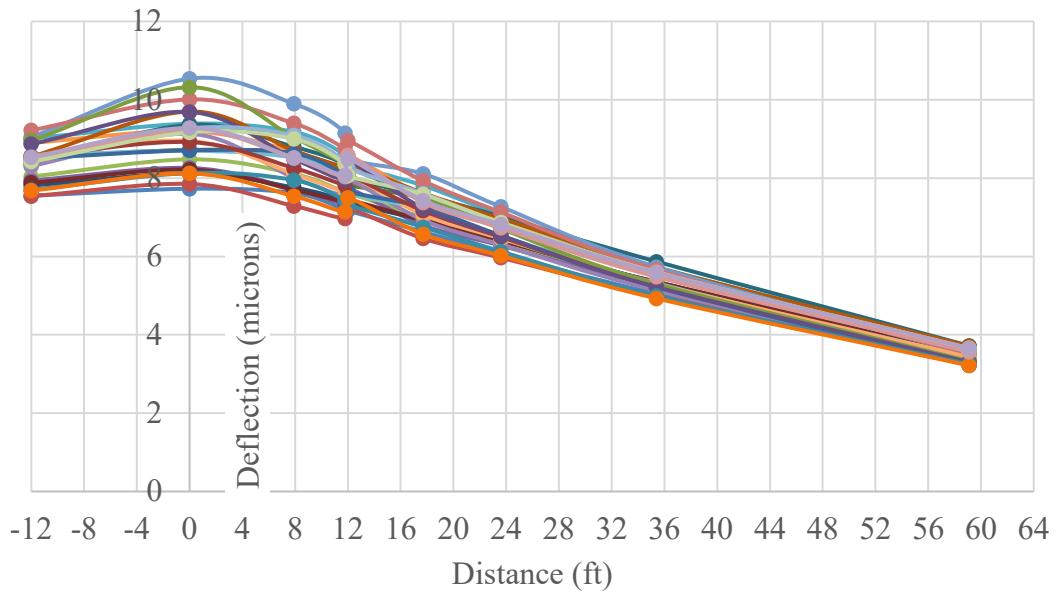


Figure 54. LTE (%) at Cell 3 (Stress 80-81 psi)



- Joint-1 App. Joint-1 Leave Joint-2 App. Joint-2 Leave Joint-3 App. Joint-3 Leave Joint-4 App.
- Joint-4 Leave Joint-5 App. Joint-5 Leave Joint-6 App. Joint-6 Leave Joint-7 App. Joint-7 Leave
- Joint-8 App. Joint-8 Leave Joint-9 App. Joint-9 Leave Joint-10 App. Joint-10 Leave Joint-11 App.
- Joint-11 Leave Joint-12 App. Joint-12 Leave Joint-13 App. Joint-13 Leave Joint-14 App. Joint-14 Leave

Figure 55. FWD Deflections at Cell 3 (Stress 107-109 psi)

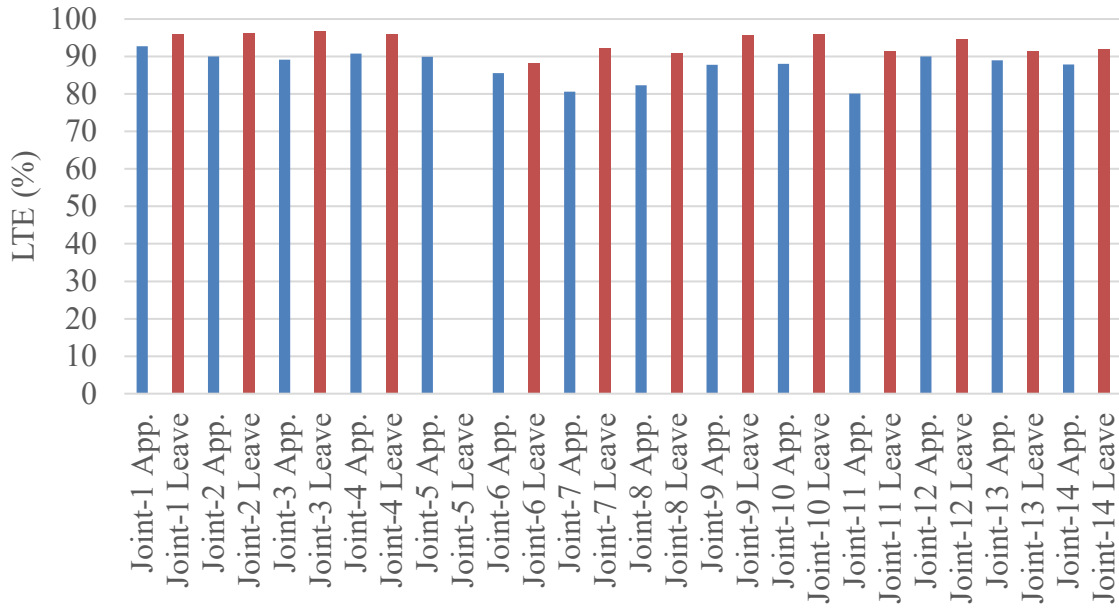


Figure 56. LTE (%) at Cell 3 (Stress 107-109 psi)

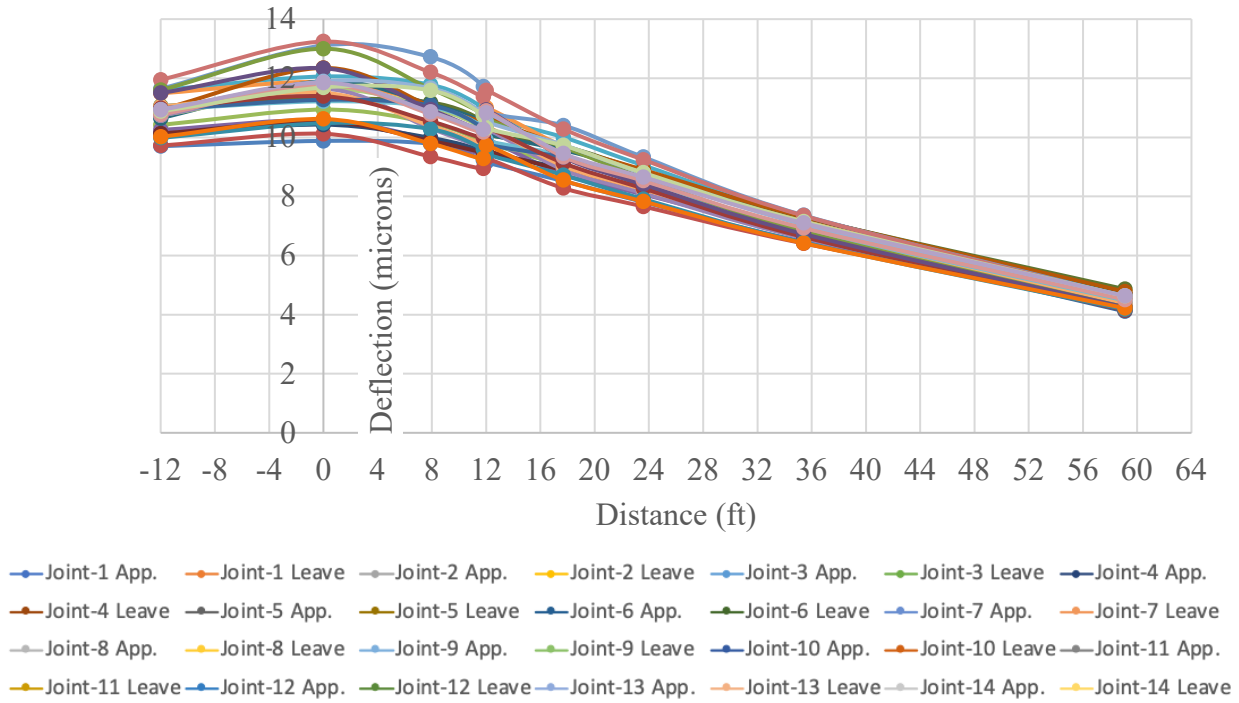


Figure 57. FWD Deflections at Cell 3 (Stress 140-142 psi)

The FWD was also used to determine the degree of interlock between adjacent slabs of the CCP. This degree of interlock is generally known as “load transfer efficiency” or LTE. Measurement of the LTE was obtained by placing the FWD load plate tangent to one side of the joint to be evaluated. A load pulse was then generated, and the deflections at equal distances on either side of the joint were measured. The results in Figure 58 show that the LTE factor varied between 90% and 100%. The LTE factor at leave stations was always higher and close to 100% compared to the approach stations. In a perfectly efficient joint, these deflections are almost equal. For most joints, the deflection on the unloaded slab is less than the deflection on the loaded slab.

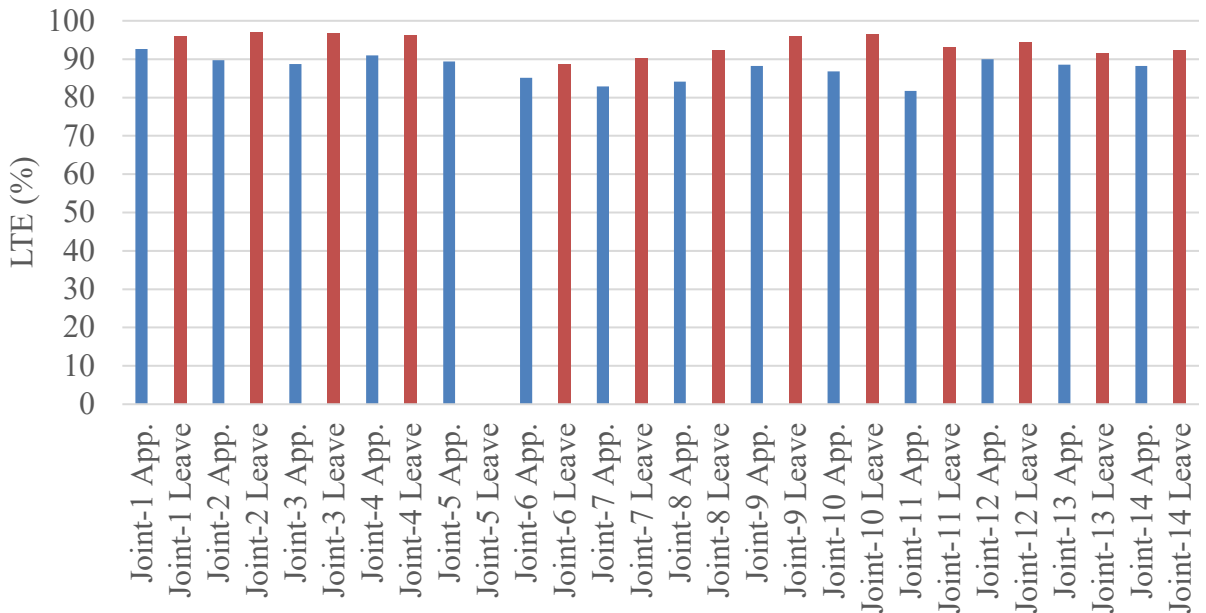


Figure 58. LTE (%) at Cell 3 (Stress 140-142 psi)

5.3 Truck Loading Test

The truck loading test was conducted by Missouri S&T on Cells 1, 2, and 3 to investigate the effect of fibers on performance of CCP. The cells were instrumented using a typical set of sensors embedded at each of the three stations. The sensors included dynamic strain gauges, two

vibrating wire gauges aligned in the longitudinal and the transverse directions, as well as two thermocouples located at the top and the bottom of the CCP slab section.

Figure 59 provides a schematic of the truckload configuration. The truck loading test was conducted under a static condition as well as at slow-moving mode (5 mph) and high-speed modes (10 and 20 mph). The static loading consisted of positioning the front wheel of the truck on top of the sensors to simulate the effect of static single axle loading. After the deformation was registered, the truck was moved forward to have the tires of the rear tandem axle being positioned on sensor spots. To investigate the effect of speed on the pavement deformations, the truck was then passed over the marked sensor locations at different speeds varying from a slow crawling speed of 5 mph to 20 mph.

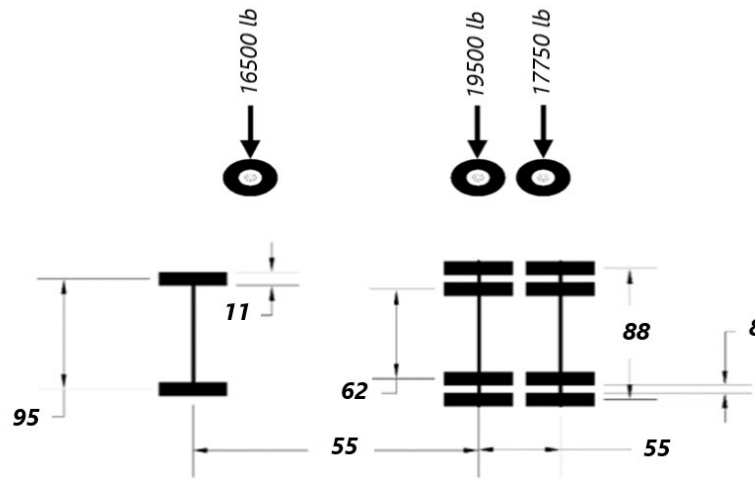


Figure 59. Schematic of truckload configuration, dimensions in inch

Table 14 shows the key parameters that were collected from the truck before the truck loading test on the testing day. The contact pressure was calculated as the axle weight over the contact area between the tires and the pavement surface.

Table 14. Axle weights and pressure at tire-pavement contact area (driver side)

Axle type	Single	Tandem	
Tire position	Front tire	Front tires	Rear tires
Tire load (lb)	16,500	19,500	17,750
Contact pressure (psi)	141	196	179

For all loading scenarios, the tires at the driver side were considered the wheel plane over the dynamic strain sensors for load testing. In the case of the tandem axle, the tires at the passenger side were placed on top of the sensors. The weights of both the driver and passenger sides of the front and the rear axles were determined in a weigh station. Figure 60 shows the loaded truck at the weigh station.



Figure 60. Truck at the weigh station

Before conducting the truck load testing, a deep metal scanner was used for detecting the exact sensors' locations, then the locations were marked to make sure that the truck wheels were placed on top of the sensors during testing. All four dynamic strain sensors for each cell were connected to jumpers according to the schematic strain gauge wiring plan provided by MnDOT. Figure 61 shows the connection of four sensors to the jumper. Trial tests were conducted by placing the tires at the passenger side on top of the marked sensor locations. Figure 62 shows the truck passing over the marked sensor locations at a constant speed.

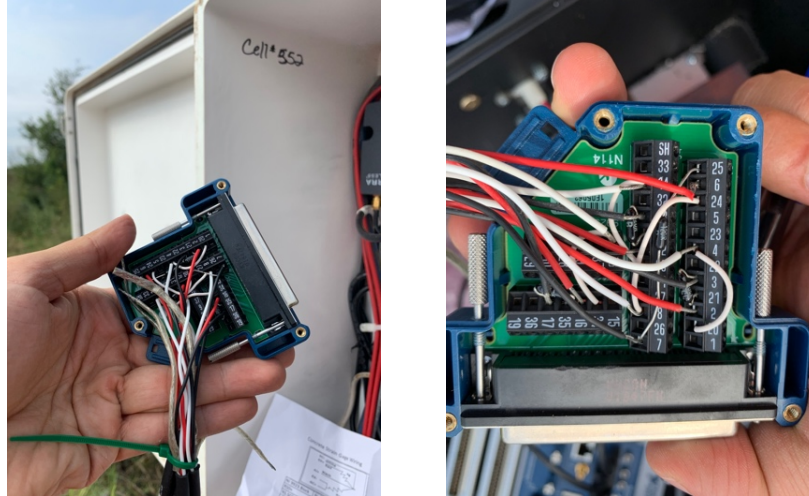


Figure 61. Connection of sensors to jumper (picture shows connections for Cell 2)



Figure 62. Truck loading test

The collected data showed that only two sensors were responsive to the truck loading test. A decision was made with MoDOT and MnRoad to conduct the truck loading test again. The first truck loading test was done on August 27th, 2020, and the second one was conducted on September 16th, 2020. For the second test, the resistance of the dynamic strain sensors (CE001, CE002, CE003, and CE004) was measured using an ohmmeter to assess the soundness of the sensors. Figure 64 shows the process of measurement of the resistance.



Figure 63. Measurement of the sensors' resistance prior to testing

Table 15 summarizes the resistance recorded for each sensor at the three cells. According to instructions from MnDOT, the settings of the Data Acquisition System (DAQ) were adjusted to widen min/max signal input range of DAQ. Table 16 lists the DAQ setting for Cells 1, 2, and 3.

Table 15. Resistance of sensors (CE001, CE002, CE003, and CE004) for Cells 1, 2, and 3

Cell 1 CE001		Cell 1 CE002	
Black to white	1.6 ohms	Black to white	1.5 ohms
Red to Black	127 ohms	Red to Black	121.3 ohms
Red to White	127 ohms	Red to White	121.3 ohms
Cell 1 CE003		Cell 1 CE004	
Black to White	1.7 ohms	Black to White	1.6 ohms
Red to Black	127.4 ohms	Red to Black	126.5 ohms
Red to White	127.4 ohms	Red to Black	126.6 ohms
Cell 2 CE001		Cell 2 CE002	
Black to White	1.5 ohms	Black to White	1.5 ohms
Red to Black	128 ohms	Red to Black	134.8 ohms
Red to White	128 ohms	Red to White	134.8 ohms
Cell 2 CE003		Cell 2 CE004	
Black to White	1.5 ohms	Black to White	1.7 ohms
Red to Black	127.3 ohms	Red to Black	126.3 ohms
Red to White	127 ohms	Red to White	126.4 ohms
Cell 3 CE001		Cell 3 CE002	
Black to White	1.2 ohms	Black to White	1.7 ohms
Red to Black	129 ohms	Red to Black	128 ohms
Red to White	129 ohms	Red to White	128 ohms
Cell 3 CE003		Cell 3 CE004	
Black to White	1.7 ohms	Black to White	1.8 ohms
Red to Black	124.8 ohms	Red to Black	130 ohms
Red to White	124.8 ohms	Red to White	130 ohms

Table 16. Adjusted Data Acquisition System setting based on resistance of sensors

Cell	Signal input range		Gage factor	Gage resistance	Lead resistance
	min	max			
551	-8k	8k	2	120	1.6
552	-8k	8k	2	120	1.6
553	-8k	8k	2	120	1.6

However, the data from the second trial confirmed that 10 out of the 12 embedded sensors were non-responsive. In general, normal at rest readings should be 120 ohms plus the lead wire resistance. Sensors with readings close to or exceeding 130 ohms are likely considered unusable. After discussion with MnDOT and MoDOT engineers, it was felt that the damage of the sensors can correspond to the compaction during the paving operations that led to excessive pressure on the sensors. Table 17 shows the values that were collected by the DAQ for the inactive sensors that show excessive amount of pressure they received during paving.

Table 17. Value ranges recorded for non-responsive sensors

Cell	CE001	CE002	CE003	CE004
1	54145.83*	21728.19	54151.31*	54165.77*
2	54145.83*	49016.3*	54151.31*	54165.77*
3	54145.83*	54170.56*	37304.72	54165.77*

* denotes non-responsive sensors

Figures 64 and 65 show variations in strain during the truck movement for Cells 1 (mixture without fiber) and 3 (mixture with fiber). The size of cells was identical at width of 24 ft, length of 12 or 15 ft, and thickness of 6 in. each.

The results of the responsive sensors indicate that Cell 3 showed relatively higher range of strain values (up to 60 $\mu\epsilon$) when the speed increased to 10 mph. The strain under static load was 50 $\mu\epsilon$. These values were limited to 45 $\mu\epsilon$ under different speed scenarios and the strain recorded

for Cell 1 was $30 \mu\epsilon$ under static load. The limited results that were obtained showed that fibers did not have any significant effect on the CCP slabs under dynamic loads.

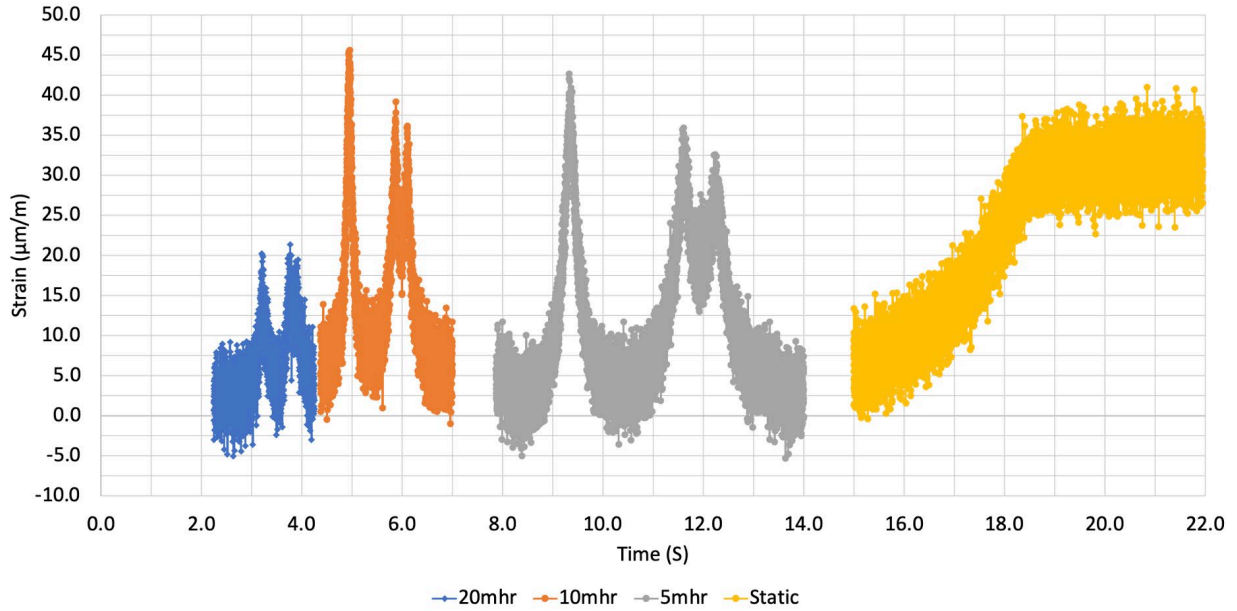


Figure 64. Variations in strain during the truck movement – bottom part of Pavement (Cell 1 with fiber)

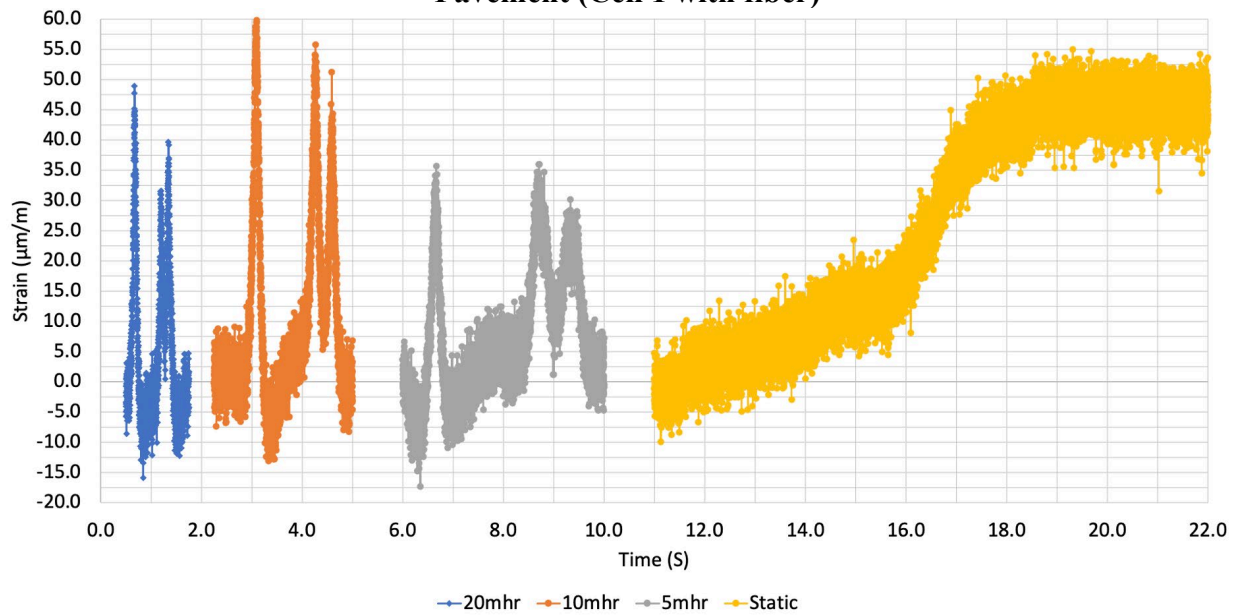


Figure 65. Variations in strain during the truck movement – bottom part of Pavement (Cell 3 with fiber)

5.4 Environmental Performance (Analysis of MnDOT Data)

The analysis of MnDOT environmental data, including the readings of three typical sets of sensors located at three different stations (551, 552, and 553) associated to Cells 1, 2, and 3, respectively, was conducted. The sensors include two vibrating wire gauges aligned in the longitudinal and the transverse directions as well as two thermocouples located at the top and the bottom of the CCP slab section (see Figure 9). The analysis of MnDOT environmental data was conducted in December 2019, June 2020, December 2020, and June 2021.

The adjusted temperature readings of the thermistors (XV) attached to the top and the bottom of the slab section at the three investigated stations 551, 552, and 553 are plotted separately in Figures 66, 67, and 68, and combined in Figure 69. The thermocouples readings at the top section of the three stations were referred to as XV 551-1, XV 552-1, and XV 553-1, while the bottom readings of the three stations were referred to as XV 551-2, XV 552-2, and XV 553-2. During the winter, the temperature varied between -2°C and 22°C , reaching its maximum value after approximately 24 hours of concrete placement. During summers, the temperature varied between 25°C and 45°C , reaching its maximum value at around the first week of August. The temperature variation between the top and the bottom of the slab was not significant, where a maximum temperature variation of less than 5°C was recorded in August 2020 at station 551. Overlap of data associated with the top and the bottom sensors of Cell 2 and Cell 3 was observed (Figures 67 and 68). The temperature started increasing again to reach values between 28 and 45°C in June 2020. During the winter of 2021, the temperature varied between -7 and 20°C and then increased again to reach values between 28 and 48°C in June 2021.

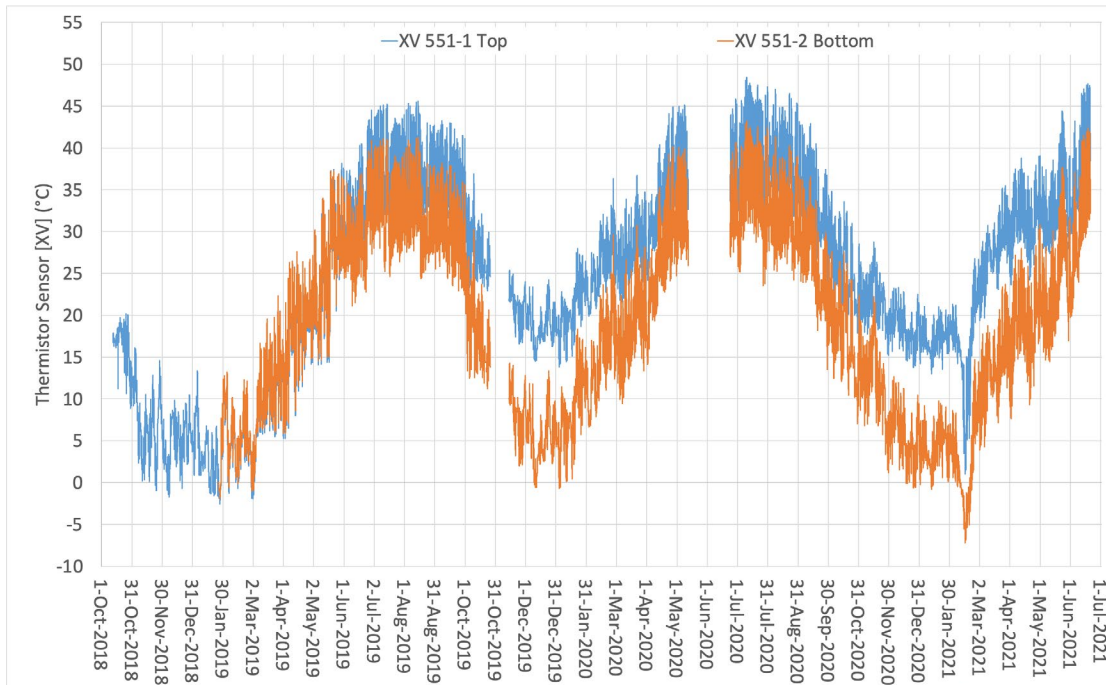


Figure 66. Temperature readings of the thermistors attached to the top and bottom of the slab section at station 551 (Cell 1)

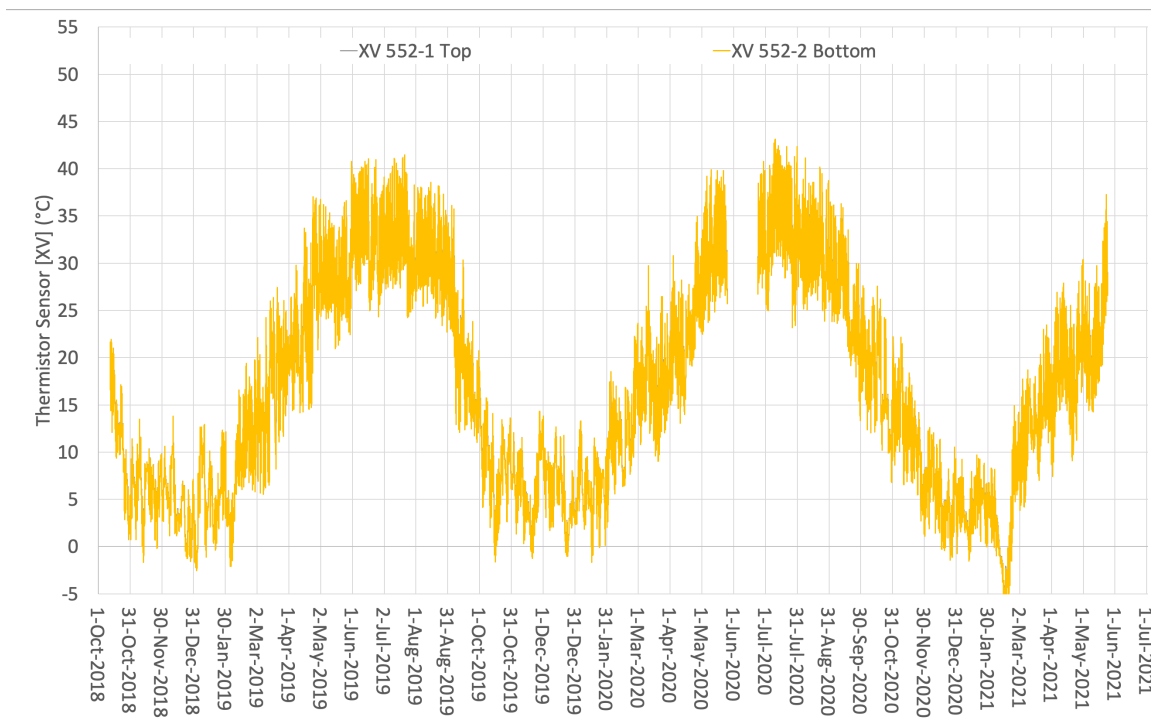


Figure 67. Temperature readings of the thermistors attached to the top and bottom of the slab section at station 552 (Cell 2)

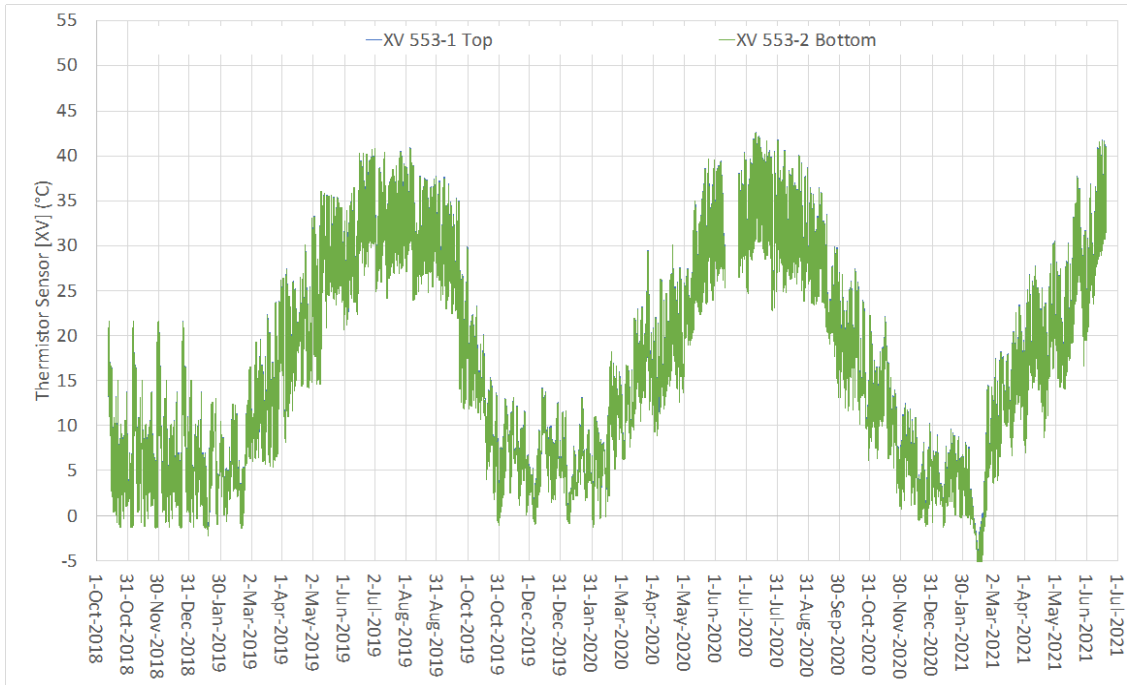


Figure 68. Temperature readings of the thermistors attached to the top and bottom of the slab section at station 553 (Cell 3)

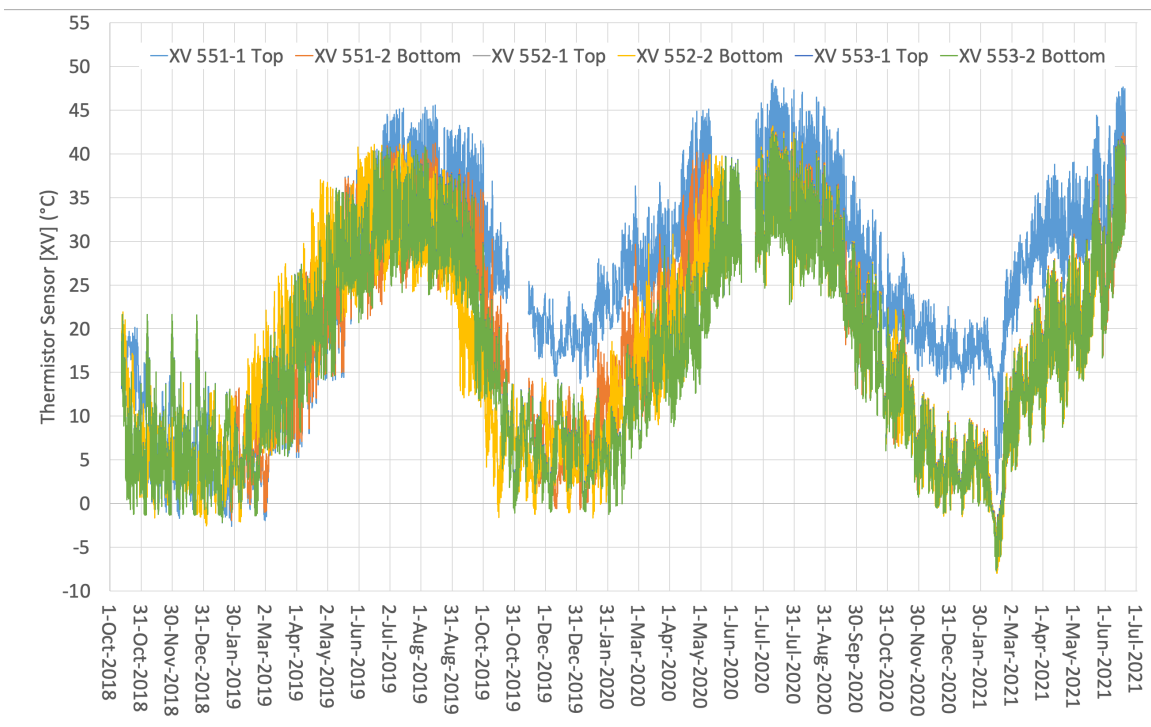


Figure 69. Temperature readings of the thermistors attached to the top and the bottom of the slab section at the three investigated stations

Figure 70 shows the strain variations of the longitudinal and the transverse directions of the investigated three stations that were referred to as VW 551-1, VW 551-2, VW 552-1, VW 552-2, VW 553-1, and VW 553-2, respectively. After approximately seven weeks of concrete placement, the longitudinal and the transverse sections reached a maximum strain of 960 and 940 $\mu\epsilon$, respectively. Generally, the strain varied between 850 and 960 $\mu\epsilon$. Both longitudinal and transverse strains went down in the summer period, reaching the lowest values in the first week of July. The strains after that started to increase. The rate of decrease of the transverse strain was much lower than the longitudinal strain. For example, at Cell 1 (Station 551), the longitudinal strain was higher than the transverse strain in the first week of May, then the transverse strain started to be higher than the longitudinal one. Strains began to decrease again starting from January 2020 and up to June 2020 to reach values similar to those of June 2019. The strains again went up to reach peak values between 932 and 962 $\mu\epsilon$ in March 2021, and like previous years strains started to go down again at the end of March to reach the lowest values in June/July 2021.

The use of fibers and variation of slab length did not have a significant effect on the environmental strain where the difference in the longitudinal and transverse strains at the three cells did not exceed 4% and 2%, respectively. Slab prepared with fibers exhibited 4% less longitudinal strain and 2% less transverse strain compared to the slab made with no fibers and having the same width of 15 ft.

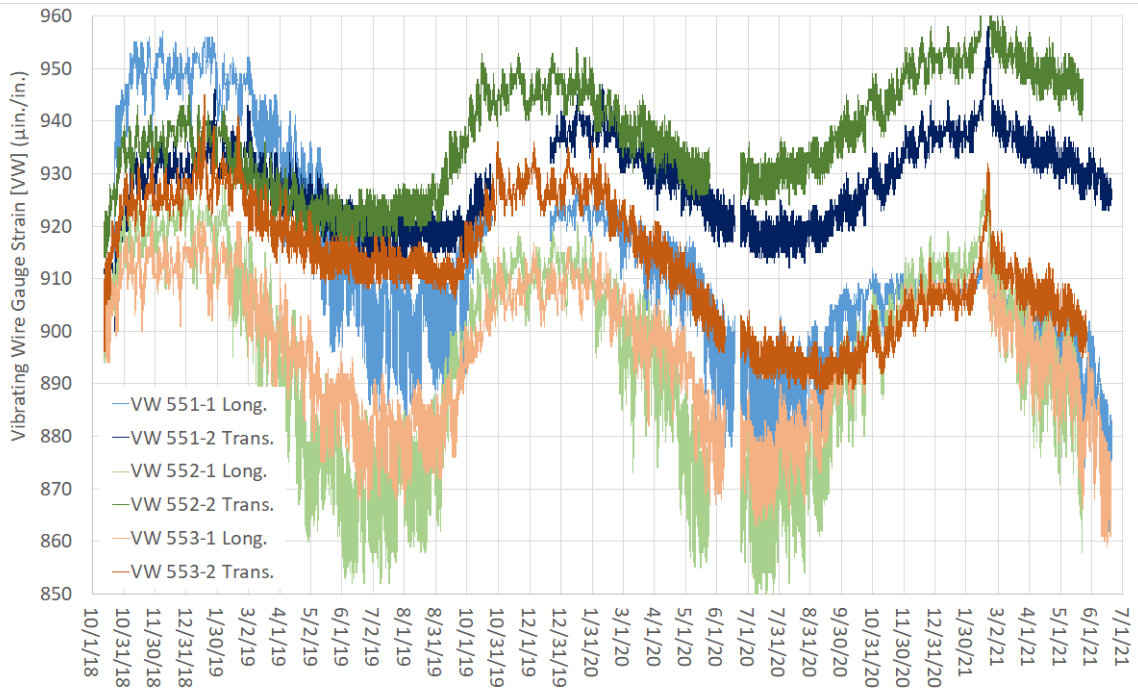


Figure 70. Strain variations at the longitudinal and the transverse directions of the three investigated stations

6 CONCLUDING REMARKS

The main objective of this project was to evaluate construction issues and characterize the long-term performance of CCP. Three CCP test cells were designed and constructed in Scott County, Missouri, as part of a larger construction project. Cell 1 and Cell 2 were prepared with no fibers and had a length of 15 ft and 12 ft, respectively. Cell 3 was prepared with fibers and had a length of 15 ft. The performance of designed CCP mixtures prepared with and without fibers were evaluated using cast-in-field and saw-cut/cored samples. The primary performance characteristics included mechanical properties, drying shrinkage, and durability, and the enhancement gained from fiber-reinforcement was assessed. Curling warping measurements were conducted periodically to assess the effect of fiber reinforcement on the deflection of three designated cells. The pavement quality after construction was monitored using truck loading and FWD. The analysis of MnDOT environmental data including the readings of three typical sets of embedded sensors located at cells was conducted. Based on the results presented in this study, the following concluding remarks can be made.

1. Based on the Vebe consistency time results for representative samples, both tested CCP mixtures made with and without fibers are categorized to have extremely dry consistency that are difficult to ensure full consolidation. The test results showed that the incorporation of fibers increased the density of the fresh CCP by 15%. It is important to note that this greater density is observed under high energy of consolidation in the Vebe test, which may not be the case in the constructed pavement sections.
2. The compressive strength of the mixture made with 5 pcy synthetic fiber was greater than that of samples made without fiber.

3. The degree of compaction was higher in cast-in-field samples than in-situ samples. For example, the 91-d compressive strength of cast-in-field samples of Mixtures 1 and 2 was approximately 40% greater than that of core specimens.
4. The use of 5 pcy of synthetic fiber slightly increased the flexural strength for cast-in-field samples but reduced that for saw-cut samples. The incorporation of 5 pcy fibers improved post-cracking behavior.
5. The use of synthetic fibers resulted in 5% and 15% decrease in the bulk and surface electricity resistivity, respectively.
6. Mixtures made with 5 pcy fiber had an air content of 5.1% compared to 4.0% for plain mixture. Mixtures prepared with and without fiber had a similar freezing-and-thawing durability.
7. No visible scaling was observed during 80 cycles indicating acceptable resistance of the two mixtures to salt scaling.
8. The incorporation of 5 pcy of fibers restricted shrinkage. The non-fibrous mixture had drying shrinkage of 1125 $\mu\epsilon$, compared to 900 $\mu\epsilon$ in the case of mixture with fibers.
9. The curling and warping in the pavement sections increased with time. No significant difference in deflection was observed between fiber-reinforced and non-fiber reinforced concrete cells.
10. The FWD test results showed that the deflection values at Cell 3 (CCP with fiber) were higher than the other two cells where concrete was prepared without any fibers. Higher deflection of the Cell 3 can be due to the voids that were formed in the interfacial transition zone of fibers or can refer to the weak subgrade support. The use of fibers can also hinder the degree of compaction of the CCP.

11. The truck loading tests results cannot be conclusive as the mortality rate of sensors was high. However, the results of the responsive sensors indicated that Cell 3 (CCP with fiber) showed relatively higher range of strain values (up to $60 \mu\epsilon$) when the speed increased to 10 mph. The strain under static load for Cell 3 was $50 \mu\epsilon$. These values were limited to $45 \mu\epsilon$ under different speed scenarios and the strain recorded for Cell 1 was $30 \mu\epsilon$ under static load. The limited results that were obtained showed that fibers did not have any significant effect on the CCP slabs under dynamic loads.
12. Environmental analysis showed that longitudinal and transverse strains decreased during the summer, reaching the lowest values in the first week of July. The rate of decrease of the transverse strain was much lower than the longitudinal strain. The use of fiber did not have a significant effect on deformations induced by environmental factors.
13. In general, test results showed that the incorporation of fibers enhanced the mechanical properties (compressive and flexural strengths) of CCP mixtures when proper compaction was provided, as in the case of cast-in field samples. Also, fibers changed the flexural failure mode of saw-cut and cast-in-field CCP samples from brittle to ductile failure. The incorporation of fibers had a restraining effect on the drying shrinkage of CCP mixtures. The use of fibers did not have a significant effect on the performance of CCP mixtures, as shown from the FWD, truck loading tests and curling and warping results. This can be mainly related to the extremely dry consistency of the CCP mixtures (Vebe consistency > 60) that can hinder bond strength in the interfacial transition zone with the matrix. This was more accentuated in the saw-cut samples from the paved CCP as the paving process in the field did not provide enough compaction. As for the size of slabs, results showed that the size of CCP slabs was more effective in the curling and warping measurements. The

slab with longer length (15 ft) showed higher variations in curing and warping along the diagonal, transverse and longitudinal lengths over time. Therefore, the use of fibers in CCP can be recommended provided that the CCP mixture has adequate workability and sufficient compaction energy applied during construction.

REFERENCES

Khayat, K.H. and Libre, N.A., 2014. Roller Compacted Concrete: Field Evaluation and Mixture Optimization. Center for Transportation Infrastructure and Safety/NUTC Program, Missouri University of Science and Technology.

ASTM C1170-91 (1998). Standard Test Methods for Determining Consistency and Density of Roller-Compacted Concrete Using a Vibrating Table, American Society for Testing and Materials.

ASTM C31, C31M (2003). Standard Practice for Making and Curing Concrete Test Specimens in the Field, American Society for Testing and Materials.

ASTM C 39 (2012). Standard Test Method for Compressive Strength of Cylindrical Concrete Specimens, American Society for Testing and Materials.

ASTM C 1609 (2012). Standard Test Method for Flexural Performance of Fiber-Reinforced Concrete (using Beam with Third-Point Loading) , American Society for Testing and Materials.

ASTM C1202 (2000). Electrical Indication of Concrete's Ability to Resist Chloride Ion Penetration, American Society for Testing and Materials.

AASHTO T95 (2013). Determining Asphalt Binder Bond Strength by Means of the Asphalt Bond Strength (ABS) Test. American Association of State and Highway Transportation Officials.

ASTM C 457 (1991). Standard Test Method for Microscopical Determination of Parameters of the Air-Void System in Hardened Concrete, American Society for Testing and Materials.

ASTM C 666/C666M-03 (2008). Standard Test Method for Resistance of Concrete to Rapid Freezing and Thawing, American Society for Testing and Materials.

ASTM C 672-98 (2001). Standard Test Method Scaling Resistance of Concrete Surfaces Exposed to De-icing Chemicals, American Society for Testing and Materials.

ASTM C157 (2006). Standard Test Method for Length Change of Hardened Hydraulic-Cement Mortar and Concrete, American Society for Testing and Materials.

ASTM E1364-95 (2017). Standard Test Method for Measuring Road Roughness by Static Level Method, American Society for Testing and Materials.